THE PROCEEDINGS OF
THE PHYSICAL SOCIETY

Section B

VOL. 65, PART 6 | 1 June 1952 | No. 390 B

Further Results in the General Theory of Barrier Layer Rectifiers

BY P. T. LANDSBERG
Department of Natural Philosophy, The University, Aberdeen

MS. received 27th September 1951, and in final form 7th January 1952

ABSTRACT. It is pointed out that the temperature variation $V_D = a - bT$ of the diffusion potential, as deduced from the forward characteristic of rectifiers, is in broad agreement with theory. Hence formulae are derived for the temperature variation of the zero resistance of a rectifier having an arbitrary distribution of impurity centres, and subject to either diode or diffusion theory. Interpretation of experiments with the aid of these formulae leads to the temperature dependence of (*a*) the effective mass of current carriers in germanium rectifiers, and (*b*) of the mobility of current carriers in selenium rectifiers. The latter curve has the same form as that obtained from Hall effect measurement, and it is pointed out that it is of broadly the same shape as the corresponding curves for high resistivity samples of silicon and germanium. It is shown that two d.c. characteristics of the same rectifier, but corresponding to different temperatures, can intersect. Formulae for the applied voltage and the temperature rise which lead to the onset of thermal instability are deduced for all impurity centre distributions, and for diode and diffusion theory. A general theory of current creep in rectifiers is outlined, and good agreement obtained with experiments on selenium rectifiers.

§1. INTRODUCTION

THE general theory of barrier layer rectifiers has been introduced so that a single analysis can cover all likely impurity centre distributions in the semiconductor. The theory can be applied to experimental material of considerable variety. There seems to be little point, however, in attempting an exhaustive enumeration of possible applications, since these should become evident as new experimental material becomes available. It may perhaps be of interest, however, to discuss matters (described by the headings of the six succeeding sections) which have recently been the subject of enquiry from the point of view of this general theory, and in this way to carry them somewhat further.

The notation introduced previously (Landsberg 1951 b, c; these papers will be referred to as I and II respectively) will be adopted.

§ 2. THE TEMPERATURE DEPENDENCE OF BARRIER HEIGHT AND RECTIFIER RESISTANCE

Consider a barrier layer having an arbitrary distribution $n(x)$ of fixed space charge. The potential energy of a current carrier in the barrier has its maximum at a plane whose distance b from the contact is given by (II, eqn. (6))

$$\frac{1}{b^2} = 16\pi \int_b^d n(x)\,dx - \frac{4\epsilon}{e^2} V'(d). \qquad \ldots\ldots(1)$$

The coordinate $x=d$ marks the end of the barrier and ϵ is the dielectric constant of the bulk semiconductor. The current density j flowing through the barrier when the voltage $U/\boldsymbol{e}$ is applied is given in diffusion theory by (II, eqn. (11))

$$\left.\begin{aligned} j &= j_0 y^{3/2} e^y (1 - e^{U/\boldsymbol{kT}}), \text{ where } y = e^2/2\epsilon b \boldsymbol{kT} \\ \text{and} \qquad j_0 &= \left(\frac{2}{\pi}\right)^{1/2} n(d) v \epsilon \left(\frac{\boldsymbol{kT}}{e}\right)^2 \exp\left(-\frac{V_D}{\boldsymbol{kT}}\right) \end{aligned}\right\} \qquad \ldots\ldots(2)$$

for reverse and very small forward potentials. For the forward direction U is positive and j is negative since the current flows in the direction of the negative x axis. For the reverse direction U is negative and j is positive.

If b_0 be the value of b when $U=0$, then the corresponding maximum potential energy in the barrier is (II, eqn. (7))

$$V(b_0) = V_D - e^2/2\epsilon b_0. \qquad \ldots\ldots(3)$$

It is easily shown that

$$-\left(\frac{dj}{dU}\right)_{U=0} = \frac{evn(d)}{2(\pi\epsilon \boldsymbol{kT} b_0^3)^{1/2}} \exp\left[-\frac{V(b_0)}{\boldsymbol{kT}}\right]. \qquad \ldots\ldots(4)$$

The ratio $|dU/dj|_{U=0}\,(=R,$ say) is sometimes referred to as the zero resistance of the rectifier, and its variation with temperature should satisfy (4). Note that with the present model of fixed impurity centres b_0, and hence $V(b_0)$, are independent of temperature.

To discuss the temperature dependence of V_D, take the zero of the potential energy of the current carriers at the top of the full band for p-type semiconductors, and at the bottom of the conduction band for n-type semiconductors, assuming the energy as positive for the states in the almost full band for p-type semiconductors, and in the almost empty band for n-type semiconductors. It follows that the energy ϵ^* of the Fermi level and the energy ϵ' of the impurity levels will in general be negative in both cases. (This is discussed more fully by Landsberg (1952).) Assuming the presence of only one type of impurity (n_b centres per unit volume) and neglecting intrinsic conduction (Mott and Gurney 1940, p. 175)

$$\epsilon^* \sim \tfrac{1}{2}\epsilon' - \tfrac{1}{2} c \boldsymbol{kT}, \text{ where } c = \log(\tfrac{1}{2}\sqrt{\pi} n_0/n_b) \text{ and } n_0 = 2(2\pi m \boldsymbol{kT})^{3/2}/h^3. \quad \ldots\ldots(5)$$

If ϕ be the work function for the current carriers, the diffusion potential V_D is given by

$$V_D = \phi + \epsilon^* \sim \phi + \tfrac{1}{2}\epsilon' - \tfrac{1}{2} c \boldsymbol{kT}. \qquad \ldots\ldots(6)$$

Inserting (5) and (6) into (4) yields

$$\frac{R_2}{R_1} \sim \frac{v_1}{v_2}\left(\frac{T_1}{T_2}\right)^{1/4} \exp\left[\frac{\beta}{\boldsymbol{k}}\left(\frac{1}{T_2} - \frac{1}{T_1}\right)\right], \text{ where } \beta = \phi + \tfrac{1}{2}\epsilon' - \frac{e^2}{2\epsilon b_0}. \qquad \ldots\ldots(7)$$

The variation of c with temperature has here been taken into consideration, and suffixes denote values corresponding to different temperatures. β is approximately equal to $V(b_0)$ and independent of temperature, since experiments on

p- and n-type silicon and on n-type germanium have shown that the change in work function as these substances are heated from 200° C to 750° C is quite negligible (Smith 1949). It is therefore likely that the corresponding changes between room temperature and 200° C are also small. For rectifiers having an arbitrary distribution of impurity centres, but subject to diode theory, the equation corresponding to (7) is

$$\frac{R_2}{R_1} \sim \left(\frac{m_2}{m_1}\right)^{1/2} \left(\frac{T_1}{T_2}\right)^{1/4} \exp\left[\frac{\beta}{k}\left(\frac{1}{T_2}-\frac{1}{T_1}\right)\right], \qquad \ldots\ldots(8)$$

where m_1 and m_2 are the effective masses of the current carriers at temperatures T_1 and T_2.

Equations (5) and (6), on which these results are based, deserve further comment. The temperature variation of V_D has been inferred from forward characteristics, and laws which are approximately the same form as (6), i.e.

$$V_D = p - qT, \quad q = 12{\cdot}5[\log(n_0/n_b) - 0{\cdot}121]10^{-3} \text{ ev/°C} \qquad \ldots\ldots(6')$$

have been obtained. The equation for q is the theoretical expression obtained from (6) for room temperatures. Table 1 gives experimental results for q, all

Table 1 Values of q from Forward Characteristics

$q \times 10^3$ (ev/°C)	Substance	Observer
0·8	Silicon	Seiler 1950
4·7	Selenium	Ewels 1950*
5·9	Selenium	Cooper 1952†

* The author is indebted to Dr. H. K. Henisch for drawing attention to this reference.
† The author is indebted to Dr. R. Cooper for sending him the curve before publication.

of which would lead to $n_b \sim 10^{19}\,\text{cm}^{-3}$ if (6′) were used. This equation can, however, give only a rough approximation, for the following reasons. (i) *Surface states* would modify the result (6). But there has not so far been any need to introduce this notion into the theory of rectification used here. We merely use the experimental fact, mentioned above, regarding the negligible temperature dependence of the work functions of silicon and germanium (cf. also Markham and Miller 1949). (ii) In the case of selenium, internal barriers may complicate the situation. (iii) In the case of silicon and germanium, intrinsic conduction should be considered. Its effect is to increase the current carrier concentration, so that the Fermi level decreases more rapidly with temperature than it would in the absence of intrinsic conduction. Actual computations of the temperature dependence of the Fermi level, taking into account intrinsic conduction, show that theory can lead to slopes of the order of 10^{-3} ev/°C (Hutner, Rittner and du Pré 1950, figs. 4 and 8, Seiler 1950, fig. 3). Thus, although the inference of V_D from forward characteristics is far from certain, experiment and theory are in broad agreement that a law of the form (6′) should hold for a limited range of temperatures.

Experiments on the variation of zero resistances with temperature have recently been reported (Billig and Ridout 1951), and been interpreted on the assumption

$$R \propto \exp(V_D/kT) \qquad \ldots\ldots(9)$$

in all cases (diffusion and diode theory). As a result V_D was found to increase markedly with temperature for selenium, silicon and germanium rectifiers. These results, which do not agree with those discussed above, must be due to

the use of (9) instead of (7) and (8) in the interpretation of the experiments. It may therefore be of interest to apply these latter equations to the experimental curves.

The expression (7) has been applied to the results for the selenium rectifier using $\beta = 0{\cdot}3$ ev, and (8) to the results for the germanium rectifier, using $\beta = 0{\cdot}4$ ev, and 17° C was chosen as the standard temperature T_1 in both cases. The curves have not been extrapolated to lower temperatures, as only one experimental point is available in that region.* The results are given in figs. 1 and 2. They are to be regarded as semi-quantitative only, owing to the arbitrary choice of β, the neglect of intrinsic conduction, and the fact that thermal contraction may cause complications in the temperature dependence of the zero resistance.

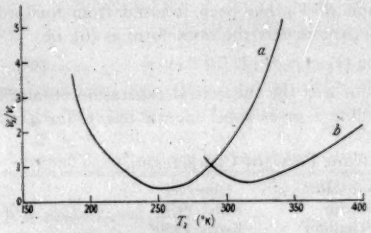

Fig. 1. Temperature dependence of the mobility of the current carriers in selenium. *a*, from the zero resistance of a selenium rectifier, *b*, from Hall effect measurements on micro-crystalline selenium.

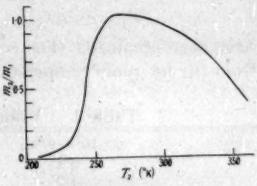

Fig. 2. Temperature dependence of the effective mass of the current carriers in a germanium rectifier from measurements of the zero resistance.

No reliable information on the temperature variation of the effective mass of current carriers in barrier layers appears to be available, but fig. 1, curve *a*, may be compared with what is known about the mobility of carriers in selenium. Mobility determinations from Hall effect measurements are somewhat uncertain, but fig. 1 appears to be in rough agreement with the results obtained by Plessner (1950) in measurements on single crystals between the temperatures 300° K and 400° K. He found an increase in the mobility by a factor of 5 in this range. The existence of a minimum in the mobility–temperature curve has also been inferred by Plessner (1951) from Hall measurements on micro-crystalline selenium, but it occurs at a higher temperature (cf. fig. 1, curve *b*). Attention has previously (I, II) been drawn to the fact that the absolute value of the mobility obtained by Henkels (1950) for micro-crystalline selenium, prepared in air, quenched, and crystallized at 110° C, was in good agreement with that obtained from rectifier characteristics. Henkels found that for this sample the mobility increased by a factor of 7·5 as the temperature was raised from 323° K to 373° K. No independent results appear to be available for selenium in the low temperature range. Such direct measurements would be of interest.

These mobility curves for selenium differ from the corresponding curves derived by Pearson and Bardeen (1949) for silicon. Most of their published mobility curves have maxima, and their shapes suggest that lattice scattering, which is proportional to $T^{-3/2}$ (Wilson 1936, p. 211, Seitz 1948), dominates at higher temperatures, while impurity scattering, which is proportional to $T^{3/2}$ (Conwell

* It appears that new and improperly understood effects occur at these lower temperatures.

and Weisskopf 1950), dominates at lower temperatures. Nevertheless, mobility curves of the selenium type have been found fairly frequently (Shockley 1950, p. 288) in high resistivity samples of silicon and germanium. Although this is not yet understood quantitatively, and selenium has a structure very different from that of silicon and germanium, the similarity between these curves should be pointed out.

§ 3. TEMPERATURE DEPENDENCE OF THE CURRENT–VOLTAGE CHARACTERISTICS

It has recently been found by Cooper (1952)* that two reverse current–voltage characteristics of the same selenium rectifier, but taken at different temperatures, may intersect. It is perhaps of interest to point out the reason for this effect.

Let suffixes 1 and 2 refer to different temperatures, and let T_1 be greater than T_2. It then follows from (2) and (3) that j_1 will be greater than, equal to, or smaller than j_2 for a fixed applied voltage (i.e. for a fixed maximum potential energy in the barrier) depending on whether

$$\frac{v_1}{v_2}\left(\frac{T_1}{T_2}\right)^{1/2} \exp\left[V(b)\left(\frac{1}{kT_2}-\frac{1}{kT_1}\right)\right] \gtrless 1.$$

Equality can therefore never occur if T_1 greater than T_2 always implies v_1 greater than v_2. In this case the higher temperature always corresponds to the higher current for all applied voltages. A necessary condition for the occurrence of the cross-over phenomenon is, therefore, that at least part of the mobility–temperature curve shall have a negative slope, as it has in selenium (cf. fig. 1). If one has two characteristics such that the one for the higher temperature corresponds also to the lower mobility, then the two characteristics will intersect at an applied voltage given by the above relation, using the equality sign.

Suppose cross-over occurs when $V(b)=V_c$. Below the cross-over voltage $V(b)>V_c$ the left-hand side becomes greater than unity, and $j_1>j_2$. Above the cross-over voltage the reverse is the case. It follows that up to the cross-over voltage the higher temperature leads to the greater current, while above the cross-over voltage the higher temperature corresponds to the lower current. These deductions, which are independent of the distribution of impurity centres in the barrier layer, explain Cooper's experimental results.

§ 4. THE GENERAL CURRENT–VOLTAGE CHARACTERISTIC

It will be shown in this section that (2) can be expressed in a different form to yield an alternative statement of the theoretical d.c. characteristics which has also received attention. It has been found (I, eqn. (13)) that for both a Mott and a Schottky barrier, and for the general class of barriers discussed in II,

$$y^r=(V_D-U)/V_0. \qquad \ldots\ldots(10)$$

V_0 and r are characteristics of a given barrier. For a Mott barrier $r=2$ and $V_0=\epsilon d k^2T^2/e^2$, where ϵ is the dielectric constant of the bulk semiconductor and d the thickness of the barrier. For a Schottky barrier $r=4$ and $V_0=\epsilon k^4T^4/8\pi n_s e^6$, where n_s is the volume density of ionized impurity centres in the barrier (cf. I and II).

Consider now all barriers for which a relation of type (10) holds. Let the reverse voltage required to depress the maximum potential energy in the barrier

* The author is indebted to Dr. R. Cooper for letting him see these results before publication.

to zero be U_C. The condition for this to happen is, by (3), that $V_D = e^2/2\epsilon b$. Hence by (2) and (10) U_C satisfies

$$V_0 = (V_D - U_C)(kT/V_D)^r. \qquad \ldots\ldots(10')$$

Using (10') to eliminate V_0 from (2), one finds

$$-\frac{j}{J} = \left(\frac{V_D - U}{V_D}\right)^{3/2r} \exp(-\overline{V}/kT)[1 - e^{U/kT}], \qquad \ldots\ldots(11)$$

where we have put

$$\overline{V} = V_D\left[1 - \left(\frac{V_D - U}{V_D - U_C}\right)^{1/r}\right] \qquad \ldots\ldots(12)$$

and

$$J = \left(\frac{2kT}{\pi}\right)^{1/2} \frac{v\epsilon n(d)}{e^2}\left(\frac{V_D^{1+1/r}}{V_D - U_C}\right)^{3/2r}. \qquad \ldots\ldots(13)$$

The quantities which occur have the following interpretation. U_C is the voltage first regarded by Sachs (1942) as the breakdown voltage of the rectifier, but its numerical values are too high for this to be the case (II, p. 481 and Landsberg 1951 c, fig. 2). $\overline{V}$ can be shown to be the maximum potential energy $V(b)$ of the current carriers in the barrier, since by (2), (3), (10) and (10')

$$V(b) = V_D - ykT = V_D - kT\left[\frac{V_D - U}{V_D - U_C}\left(\frac{V_D}{kT}\right)^r\right]^{1/r} = \overline{V}. \qquad \ldots\ldots(14)$$

Equation (11) yields, with $r = 4$, the equation used by Billig (1951 b) for a Schottky barrier, and with $r = 2$ it yields the equation used by him for a Mott barrier, provided a simple manipulation is performed and V_D is neglected compared with U_C. All characteristics of this class are therefore fully equivalent with those obtainable by using Laplace's approximation (Landsberg 1949). It should be noted, however, that (11) is somewhat less general than the original result (2), since it involves the additional assumption (10).

§ 5. THERMAL INSTABILITY OF A BARRIER HAVING AN ARBITRARY IMPURITY CENTRE DISTRIBUTION

Let T be the operating temperature of a rectifier, θ the ambient temperature, so that $\Delta T = T - \theta$ is the excess temperature. Then it has been suggested by Billig (1951 a, b) that there exists a maximum power loss per unit area per unit excess temperature which can be withstood by the rectifier. This value was assumed to be a constant $C = P/\Delta T$ for a rectifier of fixed construction and properties, which is independent of the ambient temperature. It will be shown here that the class of rectifiers for which this assumption is valid can be treated by a uniform method which covers all distributions of impurity centres.

If the ratio $P/\Delta T$ has its maximum permissible value, and the temperature is increased by an amount δT at constant applied voltage, then the current will increase, and the new power loss per unit area per unit excess temperature is

$$\frac{P}{\Delta T} + \frac{d}{d(\Delta T)}\left[\frac{P}{\Delta T}\right]\delta T.$$

The condition for thermal instability is that this new value is greater than the original (maximum permissible) value $P/\Delta T$. The condition for instability is therefore

$$\Delta T \geqslant \frac{P}{(\partial P/\partial T)_U}. \qquad \ldots\ldots(15)$$

For reverse characteristics of rectifiers (2) holds, so that

$$eP = Uj_0 y^{3/2} e^{y} \text{ (diffusion theory).} \qquad \ldots\ldots(16)$$

Using (15) and (16), one finds that the condition for instability is quite generally

$$\frac{T}{\Delta T} \leqslant \frac{V(b)}{\boldsymbol{k}T} + \frac{1}{2} + \frac{T}{v}\frac{dv}{dT}. \qquad \ldots\ldots(17)$$

This shows that *the temperature dependence of the mobility may have an important bearing on the result*. If this effect is neglected, and a Schottky barrier presupposed, (17) gives a result first obtained by Billig (1951 b, eqn. (21)). For rectifiers having an arbitrary distribution of impurity centres, but subject to the diode theory, the condition for thermal instability is different:

$$\frac{T}{\Delta T} \leqslant \frac{V(b)}{\boldsymbol{k}T} + \frac{1}{2} - \frac{T}{2m^*}\frac{dm^*}{dT}. \qquad \ldots\ldots(18)$$

The temperature variation of V_D has been neglected in these equations. Let

$$\gamma = \frac{T}{\Delta T} - \tfrac{1}{2} - D, \text{ where } D = \begin{cases} \dfrac{T}{v}\dfrac{dv}{dT} & \text{for the diffusion theory,} \\ -\dfrac{T}{2m^*}\dfrac{dm^*}{dT} & \text{for the diode theory,} \end{cases} \qquad \ldots\ldots(19)$$

then conditions (17) and (18) mean that thermal instability occurs if the temperature rise is large enough, so that $\gamma \leqslant V(b)/\boldsymbol{k}T$. Thus the Sachs criterion $V(b) = 0$ (cf. §4) is modified to

$$V(b) = \gamma \boldsymbol{k}T \qquad \ldots\ldots(20)$$

in the present model. Let the values of the parameters be distinguished by a suffix B if this condition is fulfilled. It then follows from (14) and (20) that

$$y_B = \frac{V_D}{\boldsymbol{k}T_B} - \gamma_B, \quad U_B = \frac{eC\Delta T_B}{j(y_B)}. \qquad \ldots\ldots(21)$$

Billig determined the value of U_B by a graphical method, namely, by finding the turning points of lines of constant C which cut across theoretical current–voltage curves for different temperatures. For both diode and diffusion theory, and for all impurity centre distributions, the value of U_B so determined is the same as that given by (17) and (18) (cf. Appendix). It will now be shown that the theory can be carried through analytically.

It is helpful to make the assumption (10) so that when $|U| \gg V_D$, $V_0 = (2\epsilon b/e^2)^r U(\boldsymbol{k}T)^r$. As V_0 is independent of applied voltage, and b is independent of temperature, it follows that the potential energy V_1 defined by

$$V_1^{r-1} = (e^2/2\epsilon b)^r U^{-1} \qquad \ldots\ldots(22)$$

is independent of voltage and temperature. Its values are given in table 2.

Table 2. Values of V_1 (Notation as in II)

$r=2$	Mott barrier	$V_1 = \dfrac{e^2}{\epsilon d}$.
$r=4$	General class of barriers	$V_1^3 = \dfrac{4\pi e^6}{\epsilon^3}\left(\int_b^d n\,dx\right)^2 \Big/ \int_o^d xn\,dx$.

Schottky barrier $V_1^3 = 8\pi e^6 n_s/\epsilon^3$ — Barrier introduced in II $V_1^3 = 16 e^6 n_0/\epsilon^3$

Assumption (10) leads with the notation (22) to a second equation for U_B:

$$\frac{U_B}{\boldsymbol{k}T_B} = \left(\frac{\boldsymbol{k}T_B}{V_1}\right)^{r-1} y_B{}^r. \qquad \ldots\ldots(23)$$

(22) and (23) are the two equations for the temperature T_B and the applied voltage U_B at which instability sets in. The temperature must be determined first, and is found in both diffusion and diode theory to be given by

$$(y_B \boldsymbol{k}T_B)^r j(y_B) = \boldsymbol{e}CV_1{}^{r-1}\Delta T_B. \qquad \ldots\ldots(24)$$

Introduce the notation

$$B = V_D/\boldsymbol{k}\theta,\ \tau = \Delta T/\theta,$$

$$A = \begin{cases} \left(\frac{\pi}{2}\right)^{1/2} \dfrac{\boldsymbol{e}^3 C\theta}{\epsilon v n(d)(\boldsymbol{k}\theta)^3}\left(\dfrac{V_1}{\boldsymbol{k}\theta}\right)^{r-1} & \text{for the diffusion theory,} \\ (2\pi m^*)^{1/2} \dfrac{C\theta}{n(d)(\boldsymbol{k}\theta)^{3/2}}\left(\dfrac{V_1}{\boldsymbol{k}\theta}\right)^{r-1} & \text{for the diode theory.} \end{cases} \qquad \ldots\ldots(25)$$

Substituting in (21) and (24) from the general theory of barrier layers (cf. II), and using (25), it is found that the maximum permissible temperature rise is given by

$$A = \begin{cases} \tau^{-1}(1+\tau)^{r+2}\left[\dfrac{B}{1+\tau} - \tau^{-1} - \tfrac{1}{2} + D\right]^{r+3/2} \exp\left(-\tau^{-1} - \tfrac{1}{2} + D\right) \\ \qquad\qquad \text{for the diffusion theory,} \qquad \ldots\ldots(26a) \\ \tau^{-1}(1+\tau)^{r+1/2}\left[\dfrac{B}{1+\tau} - \tau^{-1} - \tfrac{1}{2} + D\right]^{r} \exp\left(-\tau^{-1} - \tfrac{1}{2} + D\right) \\ \qquad\qquad \text{for the diode theory.} \qquad \ldots\ldots(26b) \end{cases}$$

The breakdown voltage is given by

$$U_B \frac{V_1{}^{r-1}}{(\boldsymbol{k}\theta)^r} = \left\{(1+\tau)\left[\frac{B}{1+\tau} - \tau^{-1} - \tfrac{1}{2} + D\right]\right\}^r \text{ in both theories.} \qquad \ldots\ldots(26c)$$

For a theoretical calculation it is necessary that A, B, D, $\boldsymbol{k}\theta$ and r be known. It would be useful to supplement eqns. (26) by graphical information, but this is postponed since the basic physical ideas involved are still under discussion (Cooper 1952).

Only one application of the equations (26) will be given. The three functions on the right-hand sides increase with τ unless D is negative, when they may attain a maximum and subsequently decrease. If the thermal dissipation constant is decreased, A decreases, hence τ decreases, and therefore the breakdown voltage must decrease, provided D is not negative. Cooper, however, observed an *increase* of the breakdown voltage when the thermal dissipation constant was decreased. If a theory based on thermal instability alone can account for these observations at all, then only if D can be shown to have a negative value. This shows, incidentally, that in any test of the theory it is important to take into account the temperature variation of the mobility if diffusion theory is used (or of the effective mass if the diode theory is used).

§ 6. CURVES OF CONSTANT POWER DISSIPATION

The power dissipation per unit area P and the maximum permissible temperature rise ΔT depend on several parameters: C, θ, ϵ, V_D, etc. Suppose any one of these, p^* say, is allowed to vary while all the others remain fixed,

and let suffixes 1 and 2 refer to the conditions when p^* has the values p_1^* and p_2^* respectively. Then, according to the assumption stated at the beginning of §5 (to be referred to as A), the voltages $U_1/|e|$ and $U_2/|e|$ at which thermal instability sets in are related by $P(U_1, p_1^*)/\Delta T_1 = P(U_2, p_2^*)/\Delta T_2$. If, however, the assumption of §5 is not valid, and it is more correct to assume that a certain rectifying junction can withstand only a certain maximum power loss P per unit area (this assumption is to be referred to as B), then U_1 and U_2 are related by $P(U_1, p_1^*) = P(U_2, p_2^*) = \hat{P}$. This condition yields curves of the breakdown voltage against p^* on the basis of assumption B (which must be clearly distinguished from assumption A).

Curves of this type have first been discussed for a Schottky barrier by Billig (1951 a, figs. 1 and 2, or 1951 b, figs. 7 and 8). At an ambient temperature of 17° c the value of P for the onset of thermal instability was taken as 0·92 watts/cm². The variable parameter p^* was the conductivity and the diffusion potential.† The constants used in these curves imply, when evaluated, a dielectric constant of about 19 and an impurity centre density n of about 2 to 3×10^{19} cm^{-3}. As these values are not always likely, additional curves have been calculated (figs. 3 and 4),

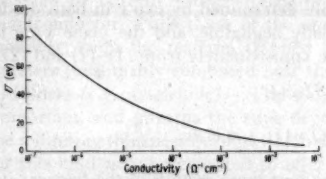

Fig. 3. Applied voltage against conductivity for constant power dissipation per unit area in a rectifier having a Schottky barrier and subject to diffusion theory.

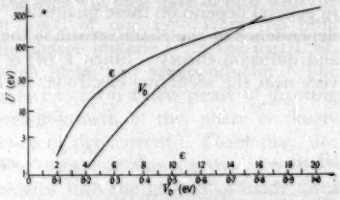

Fig. 4. Applied voltage against (*a*) diffusion potential and (*b*) dielectric constant for constant power dissipation per unit area in a rectifier having a Schottky barrier and subject to diffusion theory.

assuming a Schottky barrier and using the values (cf. I, table 2) $\epsilon = 6{\cdot}3$ (Se), $n = 1{\cdot}3 \times 10^{18}$ cm^{-3}, $kT = 1/40$ ev, $V_D = 0{\cdot}5$ ev, $P = 0{\cdot}92$ watt/cm². The last three values were also used by Billig. In fig. 3 a value of $7{\cdot}1 \times 10^{18}$ volt/cm² sec was used for the mobility (cf. I, table 2).

Another curve of constant power dissipation, based on the same constants, is added in fig. 4. It shows the important effect which the dielectric constant has on the power dissipation.

These curves are to be regarded merely as curves of the variable parameter against the applied voltage for constant power dissipation per unit area. For rectifiers for which the value of P which is required for the onset of thermal instability is 0·92 watt/cm² the applied voltage plotted must, however, be very near the breakdown voltage.

§7. THEORY OF CURRENT CREEP

Study of the time dependence of the current–voltage characteristic of selenium rectifiers (Henisch and Ewels 1950) shows that negative creep—the decrease of current with lapse of time for fixed external conditions—is met with

† There is an error in the equation on which this curve was based (Billig 1951 a, eqn. (6), 1951 b, eqn. (24)); the ratio of the diffusion potentials should be replaced by unity; this has a small effect on the curve given.

quite frequently. Positive creep can occur in selenium rectifiers for very short time intervals after the application of a voltage, and after special treatment of the rectifier a short time before the external potential is applied. Rather different phenomena occur for other rectifiers. Copper oxide rectifiers, for instance, show mainly positive creep. It is therefore desirable to go as far as possible with the general theory, and thereafter attempt special theories based on specific models.

(i) *General Theory*

Since creep occurs mainly for reverse potentials, the current density is given by

$$j = e^{y+F}, \qquad \ldots\ldots(27)$$

where y is given by (2) and

$$e^F = \begin{cases} j_0 y^{3/2} & \text{for the diffusion theory (cf. II, eqn. (10)),} \\ j_0' & \text{for the diode theory (cf. II, eqn. (13)).} \end{cases}$$

At constant temperature the current density (27) is a function of the time and of the applied voltage because the space charge distribution, and hence y, will in general depend on these quantities. The greatest part of the time and voltage dependence of the characteristic is therefore determined by $\exp y$ in both diode and diffusion theory. Since $V'(d)$ is usually negligible, and the plane $x=b$ is very near the rectifying electrode, we have approximately from (1), (2) and (27)

$$\log j = F + G\sqrt{Q}, \qquad \ldots\ldots(28)$$

where

$$G = \frac{2e(\pi e)^{1/2}}{\epsilon k T} \quad \text{and} \quad Q = |e| \int_0^d n(x)\, dx.$$

Q is the total (numerical) space charge per unit cross section of the barrier; its sign will in general be opposite to that of the predominant current carriers. As previously suggested (Landsberg 1951 a), therefore, *the problem of predicting current creep is equivalent to the problem of determining the time dependence of the total space charge Q in the barrier.* 'Positive' creep implies that Q increases with time, 'negative' creep that it decreases with time. To determine $Q(t)$, however, one must know how the thickness d of the barrier varies with time. Some information may be deduced from II, eqn. (3) (cf. also Landsberg 1951 d, Appendix B), provided the space charge distribution function, including its dependence on time, is already known.

One can go one step further in a general theory, since (Rose and Schmidt 1947)

$$\int_0^d x n(x, t)\, dx \; (= S \text{ say}) \qquad \ldots\ldots(29)$$

must remain constant for fixed external conditions. It follows that if $n(x, t)$ decreases with lapse of time at all points in the barrier, the barrier becomes thicker, while if $n(x, t)$ increases, d decreases. In particular, if n depends on x and t through two separate functions, $n(x, t) = f(x)g(t)$ say, the function g can be eliminated, since it follows that

$$n(x, t) = S \frac{f(x)}{\int_0^d x f(x)\, dx} \quad \text{and} \quad Q = |e| S \frac{\int_0^d f(x)\, dx}{\int_0^d x f(x)\, dx}. \qquad \ldots\ldots(30)$$

Both quantities depend on time through the barrier thickness. If $f(x)=x^s$,

$$Q=\frac{s+2}{s+1}\frac{|e|S}{d} \quad (s\neq -1). \qquad \ldots\ldots(31)$$

This shows the type of relation to be expected between Q and d. Thus, in general, positive creep implies decreasing barrier thickness, negative creep increasing barrier thickness.

If no new potential barriers are formed, and if parameters such as V_D and T remain unaltered, then the above results are largely independent of the physical or chemical processes which may be responsible for current creep or forming. They show that these processes are important because they lead to a modification of the total space charge $Q(t)$ in the barrier. That is why the above considerations may properly be regarded as part of what we have defined (in II) as the general theory of rectification.

(ii) *Special Theories*

No quantitative special theories are so far available. But they will have to cover at least two physically important cases. First, the case in which a new compound is formed at the contact. The theories will here have to deal with the passage of current carriers (electrons or ions) of one type from the bulk semiconductor, while those of the opposite charge migrate from the metal, or, possibly, from the material trapped between metal and semiconductor. The carriers presumably combined near the contact to form a new phase of growing thickness (e.g. a selenide). The time rate of growth of this phase is clearly important, and governs the time-dependence of the current. There may also be a limiting thickness beyond which the new substance cannot grow. Processes of this kind may be expected to offer analogies with the growth of oxide films on metals, and the special theories will therefore have to be based on what we know already about tarnishing reactions. If the new phase is relatively free from space charge, there would be a tendency for the barrier thickness to increase (by (29)). The total space charge Q in the barrier would drop due to the formation of the new compound, and increase due to an increasing barrier thickness. The general theory shows that the object of any special theory must be to estimate the importance of these two opposing trends, and hence to obtain the time dependence of Q.

The second class of physically important cases arises if the changes in the barrier can be regarded as due to forced diffusion (i.e. diffusion in the presence of a field). A tentative suggestion regarding the mechanism of current creep according to theories of this type will be offered. In it the assumption is made that the diffusion constant incorporates the effect of the electric field. This is an over-simplification, but it enables one to obtain a first insight into the problems involved.

Suppose, with Cooper (1950), that positive ions can enter the barrier in the case of a p-type semiconductor. If they do not penetrate very far, the effect of their presence on the barrier thickness may by (29) be neglected. Since the total space charge in the barrier is negative, these ions will, however, cause a decrease in the total space charge (in the semiconductor), even if they are eventually neutralized by electrons, provided only that these electrons come from the semiconductor. Ordinary diffusion theory suggests that a law of the type

$Q \propto (D_1 t)^{-1/2}$ may be valid, D_1 being an appropriate diffusion coefficient, so that (28) becomes

$$\log j = A + Bt^{-1/4}. \qquad \ldots\ldots (32)$$

Equation (32) is in agreement with creep experiments on selenium rectifiers,† as clear from fig. 5. The quantity B was found to have the value $0{\cdot}44\ \text{min}^{1/4}$ for the upper and $0{\cdot}49\ \text{min}^{1/4}$ for the lower curve.

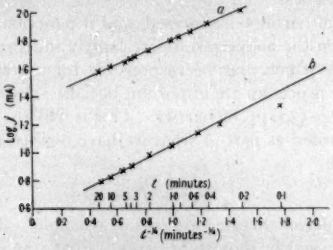

Fig. 5. Current–time curves for selenium rectifiers.
a. Specimen B2e1, $U = 16{\cdot}6$ ev, $T = 22°$ c.
b. Specimen B2b2, $U = 12{\cdot}6$ ev, $T = 19°$ c.

APPENDIX

Proof of the Equivalence of the Graphical and the Analytical Method of Determining the Onset of Thermal Instability

Consider a barrier having an arbitrary distribution of impurity centres. Diffusion and diode theory can be treated together, since the temperature dependence of the current is in both cases given by (cf. II, eqns. (11) and (13))

$$j = \alpha T^{1/2}\, e^{\beta/T}, \text{ where } -\boldsymbol{k}\beta = V_D - \boldsymbol{k}Ty = V(b). \qquad \ldots\ldots (A\,1)$$

α is temperature dependent since it involves the mobility if the diffusion theory applies, and the effective mass if the diode theory applies:

$$\alpha = \begin{cases} \text{const.} \times v \text{ (diffusion theory)}, \\ \text{const.} \times \sqrt{m^*} \text{ (diode theory)}. \end{cases} \qquad \ldots\ldots (A\,2)$$

Consider a curve of constant power dissipation $C[=jU/e(T-\theta)]$ per unit area per unit excess temperature, which cuts across current–voltage characteristics for various temperatures. For such a curve

$$\left(\frac{\partial U}{\partial j}\right)_C = \frac{eC}{j^2}\left[\frac{2T^2}{T - 2\beta + (2T^2/\alpha)(d\alpha/dT)} - (T-\theta)\right],$$

since temperature and current are related by (A 1).

Suppose $(\partial U/\partial j)_C$ is negative, i.e. the value of C can be maintained after a small rise in current only if U is correspondingly decreased. Then for phenomena which occur at constant applied voltage a small rise in current must lead to a corresponding rise in C. If C has already its maximum permissible value, however, a slight increase in current must lead to thermal instability. Similarly, if $(\partial U/\partial j)_C$ is positive, conditions are thermally stable. One finds after a short transformation that

$$\left(\frac{\partial U}{\partial j}\right)_C \lessgtr 0 \text{ if } \frac{V(b)}{\boldsymbol{k}T} \gtrless \frac{T}{\Delta T} - \frac{1}{2} - \frac{T}{\alpha}\frac{d\alpha}{dT}.$$

† The author is indebted to Drs. H. K. Henisch and J. Ewels for putting the details of their experimental results at the author's disposal.

This leads to the conditions (17) and (18) of the text, thus proving the equivalence of the graphical and the analytical method for all impurity centre distributions.

REFERENCES

BILLIG, E., 1951 a, *Proc. Phys. Soc.* B, **64**, 342 ; 1951 b, *Proc. Roy. Soc.* A, **207**, 156.
BILLIG, E., and RIDOUT, M. S., 1951, *Nature, Lond.*, **167**, 1028.
CONWELL, E., and WEISSKOPF, V. F., 1950, *Phys. Rev.*, **77**, 388.
COOPER, R., 1950, *Proc. Phys. Soc.* B, **63**, 176 ; 1952, *Proc. Phys. Soc.* B, **65**, 409.
EWELS, J., 1950, *Ph.D. Thesis*, Reading.
HENISCH, H. K., and EWELS, J., 1950, *Proc. Phys. Soc.* B, **63**, 861.
HENKELS, H. W., 1950, *Phys. Rev.*, **77**, 734.
HUTNER, R. A., RITTNER, E. S., and DU PRÉ, F. K., 1950, *Philips Res. Rep.*, **5**, 188.
LANDSBERG, P. T., 1949, *Nature, Lond.*, **164**, 967 ; 1951 a, *Proc. Phys. Soc.* B, **64**, 277 ; 1951 b, *Proc. Roy. Soc.* A, **206**, 463 ; 1951 c, *Ibid.*, **206**, 477 ; 1951 d, *Z. phys. Chem.*, **198**, 75 ; 1952, *Proc. Roy. Soc.* A, in the press.
MARKHAM, J. J., and MILLER, P. H., 1949, *Phys. Rev.*, **75**, 959.
MOTT, N. F., and GURNEY, R. W., 1940. *Electronic Processes in Ionic Crystals* (Oxford : University Press).
PEARSON, G. L., and BARDEEN, J., 1949, *Phys. Rev.*, **75**, 865.
PLESSNER, K. W., 1950, *Nature, Lond.*, **166**, 1073 ; 1951, *Proc. Phys. Soc.* B, **64**, 681.
ROSE, F., and SCHMIDT, H., 1947, *Z. Naturforsch.*, **2a**, 226.
SACHS, R. G., 1942, *N.D.R.C. Rep. No.* 14-129 (Purdue University).
SEILER, K., 1950, *Z. Naturforsch.*, **5a**, 393.
SEITZ, F., 1948, *Phys. Rev.*, **73**, 549.
SHOCKLEY, W., 1950, *Electrons and Holes in Semi-conductors* (New York : Van Nostrand).
SMITH, A. H., 1949, *Phys. Rev.*, **75**, 953.
WILSON, A. H., 1936, *Theory of Metals* (Cambridge : University Press).

Breakdown in Selenium Rectifiers

BY R. COOPER

Department of Electrical Engineering, University of Liverpool

MS. received 5*th October* 1951, *and in amended form* 16*th January* 1952

ABSTRACT. The paper describes an experimental investigation of breakdown in selenium rectifiers. Cooling from about 110°C to −74°C caused the breakdown voltage to decrease continuously, and at the same time anomalous behaviour was observed in the current–voltage characteristics. When high voltages were applied, the current decreased as the temperature increased, but at low voltages rise in temperature caused the current to increase.

The effect of changing the thermal dissipation constant was similar to that caused by a change in ambient temperature. Reduction in the dissipation constant, effected by placing the rectifier in a vacuum, was observed to *increase* the breakdown voltage, but the leakage current at low voltages also increased.

None of the available theories appears to account satisfactorily for the observations.

§ 1. INTRODUCTION

ALL contact rectifiers break down when excessive reverse voltages are applied. The phenomenon is illustrated by the current–voltage (I, V) characteristics shown in fig. 1. As the reverse voltage is increased, the differential resistance $\partial V/\partial I$ decreases and finally becomes approximately equal to the resistance of the rectifier in the conducting direction. The barrier layer has then become

ineffective, and by extrapolating the reverse characteristic in the manner shown in fig. 1 the breakdown voltage (U_c) may be determined. Breakdown in contact rectifiers must not be confused with insulation breakdown; it is not accompanied by disruption of the material between the two electrodes, and it is reversible.

Although rectifier breakdown is a phenomenon of some practical interest, there appears to be a dearth of detailed experimental facts about it. However, theories have been proposed by Sachs (1942), Schottky (1942) and Billig (1951), and their predictions are compared in this paper with the results of some experiments recently carried out by the author.

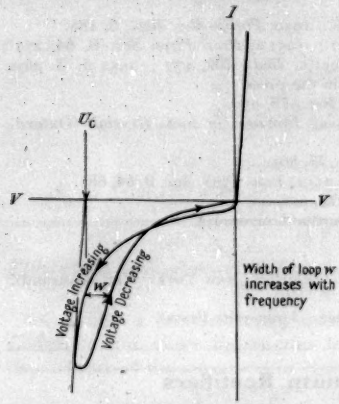

Fig. 1. Dynamic characteristic illustrating breakdown of a selenium rectifier.

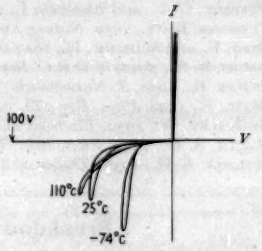

Fig. 2. Illustrating effect of ambient temperature on breakdown.

§ 2. EXPERIMENTAL

The experiments were carried out to determine how the breakdown voltage varied with ambient temperature, counter-electrode metal, and the thermal dissipation constant of the rectifier. Both commerical and fully formed laboratory prepared rectifiers were used. A vacuum evaporation method similar to that recently described by Billig (1951 b) was adopted for the preparation of the latter specimens, and spectroscopically pure materials were used.

Since Joule heating and current creep rendered it difficult to obtain reliable static I/V characteristics over an extended range of reverse voltages, breakdown was investigated by displaying dynamic characteristics on a d.c. oscilloscope. The reverse characteristics were of the form shown diagrammatically in fig. 1. The width of the two loops depended on the frequency of a.c. supplied to the measuring circuit. At 50 c/s and less the loops were not pronounced, but with increase in frequency the major loop increased considerably in width. Attention has previously been drawn by Billig (1951 b) to the existence of the major loop, but he apparently did not study the effect of frequency on it. In the present paper the values of breakdown voltages were obtained at 50 c/s from the portion of the characteristic corresponding to increasing values of reverse voltage.

The ambient temperature was varied from about 30°c to −74°c in experiments with the laboratory prepared rectifiers; in the case of the commercial rectifiers it was varied from 120°c to −74°c. At room temperature and above the rectifiers

were immersed in transformer oil. Pentane was used below 20°C. The breakdown voltage of both kinds of rectifier was found to decrease continuously with fall in temperature. The effect observed with a commercial rectifier is illustrated by the oscillograms shown in fig. 2. At 110°C the breakdown voltage was about 70 volts, at 25°C it was 50 volts, but at −74°C it was only 25 volts. The effect was reproducible, and immersion in oil at 110°C did not destroy the rectifier, despite the fact that the high temperature caused the counter-electrode to melt.

There is also apparent in fig. 2 another phenomenon of considerable interest. Comparison of the characteristics shows that whilst a rise in ambient temperature had caused the leakage current corresponding to small reverse voltages to increase, the reverse effect had occurred at voltages on the knees of the characteristics and beyond. With increase in reverse voltage the temperature coefficient ($\partial I/\partial T$ at constant voltage) had changed from positive to negative. This phenomenon occurred with both commercial and laboratory prepared rectifiers. Its existence was confirmed by applying various continuous voltages to the rectifiers and at each voltage, when the rate of current creep had become small, observing the change in current caused by a rise in temperature.

The characteristics shown in fig. 2 are consistent with the two curves published by Komar (1947) illustrating the effect of cooling a commercial selenium rectifier from room temperature to about −50°C, but they are not consistent with the characteristics given by Williams and Thompson (1941). The latter show that heating a rectifier from 20°C to 80°C caused the leakage current to increase at all voltages. Possible differences in the manufacturing processes of the rectifiers, about which little is known, may account for the difference in behaviour. A negative temperature coefficient has been observed previously in laboratory prepared rectifiers by Schmidt (1941), who obtained static reverse (I, V) characteristics up to about 1·0 volt at temperatures between 22°C and −92°C, and also by Henisch and Ewels (1950), who found that cooling a rectifier from room temperature to about −50°C with 10 volts d.c. applied caused the leakage current to increase.

The effects just described were found to be independent of the metal used as counter-electrode. But at room temperature the breakdown voltage differed considerably for different metals. Experiments were made using rectifiers with counter-electrodes of magnesium, aluminium, cadmium, bismuth, zinc and antimony. Variation was observed in the properties of apparently similar rectifiers, but the effect of counter-electrode metal on the breakdown voltage at room temperature is illustrated by the following average values : magnesium 130 v, aluminium 100 v, cadmium 60 v, bismuth 40 v, zinc and antimony about 20 v.

In a recent paper (Billig 1951 b) it has been stated that the breakdown voltage of selenium rectifiers is increased by increasing the thermal dissipation constant. This statement was not borne out by the following experiment. A commercial rectifier was suspended in a bell jar, and by means of a suitably placed valve a stream of air could be drawn over the rectifier; alternatively the bell jar could be evacuated to a pressure of about 10^{-5} mm Hg, thus changing considerably the thermal dissipation constant.

In fig. 3, curve *a* is the dynamic characteristic observed when the air stream passed over the rectifier. The temperature of its counter-electrode, measured by a thermocouple, was 28°C. Curve *b* is the dynamic characteristic observed after the air pressure in the bell jar had been reduced to about 10^{-5} mm of Hg. During the time taken to reach this pressure the voltage applied to the measuring circuit was kept constant, but the temperature of the rectifier rose above the melting

point of the counter-electrode, approximately 120°c, before thermal equilibrium was restored. The effect brought about by the considerable reduction in the thermal dissipation constant is clearly similar to that caused by increasing the ambient temperature from about 25°c to 100°c, and illustrated in fig. 2. The leakage current increased at low voltages, but breakdown occurred at a higher voltage.

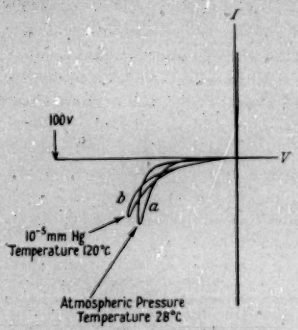

Fig. 3. Effect of change in thermal dissipation constant on breakdown.

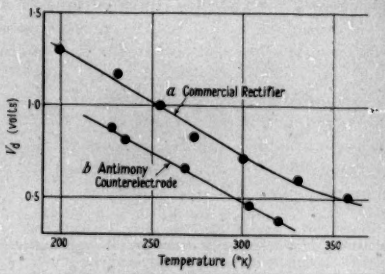

Fig. 4. Effect of temperature on V_d. Result obtained from forward (I, V) characteristics.

§3. DISCUSSION

3.1. *Image Force Theory*

Since the electric intensity in a barrier layer is estimated at about 10^5 or 10^6 v/cm, the height of the potential barrier may be influenced by image force, and Sachs (1942) has suggested that breakdown will occur when the applied voltage is sufficient to depress the height of the barrier to about the same magnitude as the average thermal energy of current carriers in the semiconductor. When this criterion is applied to the Schottky type of barrier layer, which is generally assumed to exist in selenium rectifiers, the following equation results :

$$U_c = \frac{K^3}{8\pi e^6}\frac{V_d^4}{N} \qquad \ldots\ldots(1)$$

where U_c = breakdown voltage, K = permittivity of the semiconductor, e = charge on an ionized impurity centre, N = density of charged impurity centres, V_d = height of potential barrier neglecting image force.

Landsberg (1951) has previously pointed out that when reasonable values for the parameters are inserted the value obtained for U_c is several orders of magnitude too great, but eqn. (1) is based on a very simple model of the barrier layer that might be expected to yield high values of U_c. The theory cannot be rejected for the above reason alone. However, the theory appears to be contradicted by the experiments since it apparently predicts U_c independent of temperature. But since both V_d and N may vary with temperature, the effect of possible variations in these quantities must be considered.

Equation (1) indicates that U_c is most sensitive to variations in V_d, and Billig and Ridout (1951) have deduced from the variation with temperature of the zero resistance $(\partial V/\partial I)_{V\to 0}$ that V_d rapidly decreases with fall in temperature between 20°c and −195°c. However, this result has been questioned by Landsberg (1952) who has shown that these measurements can be interpreted quite plausibly

by assuming constant V_d and temperature dependent current carrier mobility. Clearly the conclusion of Billig and Ridout cannot be accepted unless it is confirmed by an alternative method of measurement.

The variation of V_d with temperature can also be obtained from Schottky plots of (1/capacitance)^2 against bias voltage, and also by extrapolating the linear portions of the forward (I, V) characteristics back to the voltage axis. The first method is, however, not a good one. It involves extrapolating curves which, in experiments made by the author, were generally not linear ; also the capacitance of selenium rectifiers is in many cases (Cooper 1949, Joos 1948) a function of frequency, and until a satisfactory explanation of the effect is found some doubt must exist about values of V_d and N obtained by this method. However, the author is unaware of any capacitance measurements which indicate that V_d decreases with fall in temperature. The second method has the advantages that the observations require for their interpretation no formula based on a particular model of the barrier layer. Figure 4 illustrates results obtained by this method on a commercial rectifier (curve *a*) and on a laboratory prepared rectifier with a counter-electrode of antimony (curve *b*). In both cases V_d *increased* linearly with fall of temperature from 20°c to about -74°c. This result is qualitatively in agreement with the theory of Fowler (1936), but numerical agreement is not good. The contact potential difference between a metal and an exhaustion semiconductor like selenium with about 10^{17} impurity centres per cm^3 should, acccording to the theory, increase linearly only by about 0·05 ev on reducing the temperature between the above limits. The reason for this difference is not known, but errors caused by effects at grain boundaries may exist in values of V_d obtained from forward characteristics. It is, however, unlikely that they alone would account for the difference in results obtained by the two methods.

For the above reasons it cannot be assumed that V_d decreases with fall in temperature, and an appreciable increase in N must be assumed to account for the observed decrease in breakdown voltage. But capacitance measurements made by Schmidt (1941) provide no evidence of this, nor have similar measurements made by the author. However, Plessner (1951) has given reasons for believing that the density of impurity centres in micro-crystalline selenium may be increased by reducing its temperature below 20°c. But it is not certain that the material of the barrier layer possesses the same properties as the bulk Se: there is some evidence for believing a chemical compound is formed at the interface (Williams and Thompson 1941, Henisch and Ewels 1950).

It does not appear that N increases with fall in temperature, but this possibility cannot be definitely ruled out because of the sparse and unsatisfactory available evidence.

The experiments described in §2 have shown that at room temperature the breakdown voltage depends on the counter-electrode metal, and this result is qualitatively in accordance with the image force theory of breakdown.

3.2. *Schottky's Pass Effect*

Capacitance measurements on selenium rectifiers indicate that the barrier layer thickness is only equal to a few times the average separation between charged impurity centres. This led Schottky (1942) to point out that we cannot assume a continous variation in potential through the barrier layer. We must assume that it consists of a range of hills separating the neighbouring charged impurity centres. According to Schottky, enhanced current at low voltages and breakdown at higher

voltages may result from the existence of localities, called 'passes', that fortuitously contain a greater density of charged impurity centres than the average for the barrier layer. In effect a 'pass' provides a path of low resistence through the barrier layer. The magnitude of the resistance may not greatly exceed the spreading resistance of the semiconductor in series with the pass.

The theory does not allow calculation of the breakdown voltage, but a decrease in this quantity with increase in N may be expected. In this respect the theory is similar to the image force theory, and the possibility of N increasing with fall in temperature has been discussed.

3.3. *Thermal Instability*

Breakdown in rectifiers may occur (Billig 1951 a, b), provided the temperature coefficient is positive, when the heat generated per sec per °c above ambient exceeds that dissipated per sec per °c above ambient by the cooling arrangement. But the rectifiers used for the experiments described in this paper possessed a negative temperature coefficient at voltages on and beyond the knee of the (I, V) characteristic, and for this reason breakdown cannot be attributed to thermal instability. For the same reason the loop in the breakdown portion of the dynamic (I, V) characteristics cannot be accounted for in the manner suggested by Billig (1951 b).

§4. CONCLUSIONS

The experiments have shown that breakdown may occur in selenium rectifiers at higher voltages as the ambient temperature is raised, and as the thermal dissipation constant is lowered. At low voltages the temperature coefficient is positive, but near to and beyond the knee of the (I, V) characteristic it is negative.

The results do not support the thermal instability theory of breakdown. The other theories cannot be ruled out because not enough is known about the variation with temperature of the density of charged impurity centres in the barrier layers.

ACKNOWLEDGMENTS

The work described has been carried out in the Electronics Laboratories of Liverpool University, but the author's interest in the subject was first aroused some time ago at A.E.I. Research Laboratory, Aldermaston. He would like to acknowledge the liberal opportunities which he was given there to familiarize himself with the problems of contact rectification. He also wishes to thank one of his former A.E.I. colleagues, Dr. P. T. Landsberg, now at Aberdeen University, for many stimulating discussions on breakdown, and Miss J. Harrington, who has assisted with some of the experiments.

REFERENCES

Billig, E., 1951 a, *Proc. Phys. Soc.* B, **64**, 342; 1951 b, *Proc. Roy. Soc.* A, **207**, 156.
Billig, E., and Ridout, M. S., 1951, *Nature, Lond.*, **167**, 1028.
Cooper, R., 1950, *Proc. Phys. Soc.* B, **63**, 176.
Fowler, R. H., 1936, *Statistical Mechanics* (Cambridge: University Press).
Henisch, H. K., and Ewels, J., 1950, *Proc. Phys. Soc.* B, **63**, 861.
Joos, G., 1948, *Physics of Solids, FIAT Review.*
Komar, V. G., 1947, *Elecktrichestvo*, **2**, 14.
Landsberg, P. T., 1951, *Proc. Roy. Soc.* A, **206**, 477; 1952, *Proc. Phys. Soc.* B, **65**, 397.
Plessner, K. W., 1951, *Proc. Phys. Soc.* B, **64**, 68.
Sachs, P. G., 1942, *N.D.R.C. Report* 14-129 (Purdue University).
Schmidt, A., 1941, *Z. Phys.*, **117**, 754.
Schottky, W., 1942, *Z. Phys.*, **118**, 539.
Williams, A. L., and Thompson, L. E., 1941, *J. Instn. Elect. Engrs.*, **88**, Pt. I, 353.

Characteristics of Scintillation Counters

By G. F. J. GARLICK and G. T. WRIGHT

Department of Physics, University of Birmingham

MS. received 12*th November* 1951, *and in amended form* 30*th January* 1952

ABSTRACT. Experimental studies have been made of the distribution in size of output pulses from a scintillation counter detecting monoenergetic alpha-particles. Separate investigations have been made of contributions to the pulse size spread by the photomultiplier and by the scintillating crystal. It is shown that the main effect is due to statistical fluctuations in the number of photoelectrons produced at the photomultiplier cathode. The effect of the multiplying stages on these fluctuations is investigated and also the effect of flaws in the detecting crystal. The frequency distribution of the pulses is usually found to follow the gaussian form.

§1. GENERAL INTRODUCTION

When a scintillation counter, comprising photomultiplier and luminescent crystal, is used to detect monoenergetic particles fluctuations occur in the magnitude of the output pulses. Several workers have made experimental and theoretical studies of such fluctuations (Engstrom 1947, Morton and Mitchell 1948, Morton 1949, Hoyt 1949). In order to determine the various sources of fluctuations, a procedure not adequately covered by the above workers, we have made separate studies of the contributions from the various stages of the photomultiplier and from the phosphor crystal under the conditions obtaining in scintillation counters. The following factors are likely to contribute to the pulse spread: (i) variation in intensity of successive light pulses arriving at the photomultiplier cathode due to local variations in light production in the crystal and to variations in light transmission from crystal to cathode, the latter arising from crystal flaws, reflection and absorption; (ii) fluctuations in the number of electrons passing through the photomultiplier due to low photoelectric response of the cathode and non-uniform response over its surface, to low electron collection efficiency in the multiplying stages and to variation in response over the dynode surfaces.

In order to investigate effects due to the photomultiplier the phosphor crystal was replaced by a neon lamp connected in a simple saw-tooth oscillator circuit. The light pulses from this source are found to be of uniform intensity and have a controllable repetition frequency. By reducing the light intensity with neutral filters, calibrated by use of a photometer with similar neon lamp source, the light pulse intensity at the photomultiplier cathode can be varied over a wide range. After investigation of photomultiplier characteristics, measurements with the phosphor crystal as light source enable the contribution of the latter to pulse variations to be determined. (Since the neon lamp light pulses are of relatively long duration, about 10 μsec, compared with scintillation pulses, the time constant of the multiplier output circuit is made large enough to integrate the pulses and so provide a true measure of total light intensity per pulse.)

§ 2. THEORETICAL INTRODUCTION

In other investigations, referred to above, a mean quantum efficiency for the whole of the photomultiplier cathode has been assumed and also a mean gain for each multiplying stage. In a detailed analysis, not included here, we have found that such average values are justified if the average photon distribution over the cathode surface remains the same for successive scintillations and if the average distribution of incident electron density on any dynode surface is the same for successive electron pulses. There is an important difference between our studies and previous investigations. Statistical considerations of other workers are developed by determining the output pulse magnitude due to single electrons leaving the photocathode, whereas in our studies the practical conditions are assumed. We therefore consider output pulse fluctuations due to any given number of photoelectrons leaving the cathode. A further difference is that Hoyt (1949) considers separately fluctuations due to the multiplying stages but considers collectively effects due to the photocathode, light collection system and phosphor crystal. It must also be pointed out that the considerable discrepancy found by Morton and Mitchell (1948), and Morton (1949), between experimental and theoretical results is due partially to a mistake in their theoretical derivations. To correct for this discrepancy they assume interstage focusing losses for electrons. However, in their calculations they use the secondary electron emission ratio of the dynodes in an expression where the mean gain per stage is what is required. As a result by later correcting for focusing losses they include the effect of such losses twice.

Following analyses similar to those of the above workers, we obtain an expression for the variance of the charge arriving at the collector electrode of the photomultiplier per scintillation as follows:

$$\frac{\overline{Q^2}-\overline{Q}^2}{e^2}=(\overline{X^2}-\overline{X}^2)p^2f^2s^{2t}+pf\overline{X}s^t\left\{\frac{s^{t+1}-1}{s-1}-pfs^t\right\}, \qquad \ldots\ldots(1)$$

where barred symbols indicate mean values, e is the electronic charge, X the number of photons produced by absorption of one monoenergetic particle in the phosphor crystal, p is the probability that a photon incident on the cathode produces an electron which enters the multiplying stages, f is the fraction of the photons produced which reach the photocathode, s is the mean gain per multiplying stage and t the number of stages. By assuming $s^{t+1}\gg 1$ and taking M as the mean gain of the multiplying stages we have

$$\frac{\overline{Q^2}-\overline{Q}^2}{e^2}=(\overline{X^2}-\overline{X}^2)p^2f^2M^2+pf\overline{X}M^2\left(\frac{s}{s-1}-pf\right). \qquad \ldots\ldots(2)$$

The first term on the right-hand side represents the contribution from the phosphor crystal. The second term is similar to that of Morton and Mitchell for the effect of the photomultiplier but it now includes the product pf in parenthesis which takes account of the efficiency with which photons originating in the crystal produce electrons which enter the multiplier. For the two types of photomultiplier examined (EMI types 4588 and 5311) and their accompanying crystal systems pf is about 0·01 and can be neglected compared with the factor $s/(s-1)$. Its small size is due to low light collection efficiency in the case of the arrangement using the 4588 type tube and to the loss of light by transmission through, and reflection from the cathode of the 5311 type multiplier.

When pulses of electrons leave the photomultiplier cathode the resulting pulse distributions are different from those due to single electrons leaving the cathode (cf. Engstrom 1947). In our experiments we find the distributions to be of gaussian form with a given half width η. The use of the usual gaussian formulae together with eqn. (2) gives the following expression for η:

$$\eta^2 = \beta(E) + \frac{K}{\overline{V}}\left(\frac{s}{s-1}\right), \qquad \ldots\ldots(3)$$

where $K = 5{\cdot}54\ e^M/c$, c being the capacity to earth of the collector electrode, $\overline{V}$ is the mean pulse voltage and $\beta(E)$ the contribution of the phosphor crystal.

§ 3. EXPERIMENTAL STUDIES

(i) *Experimental Methods*

'Integral bias curves' were obtained by feeding the output pulses from the photomultiplier into a conventional discriminator and scaler unit. To obtain the derivative of these curves directly a single channel pulse analyser of unique design was used. This apparatus, to be described elsewhere, presents the required frequency distribution as a trace on a cathode-ray tube screen which can be photographed.

When using a luminescent crystal and alpha-particle source to provide scintillations the efficiency of light collection was improved by cementing the given small crystal to the glass envelope of the photomultiplier. In the experiments to be described an EMI type 4588 multiplier was used with opaque antimony–caesium photocathode (side window entry for light) and nine stages of multiplication. However, similar results have been obtained for an EMI type 5311 multiplier. All voltage supplies were very carefully stabilized and very slow d.c. drift of the supply was also compensated. The latter is a serious disturbing factor when making observations over several minutes with a conventional scaling unit.

(ii) *The Form of the Pulse Distribution Curve*

If the pulse distribution is of gaussian form, then if $\overline{V}$ is the mean pulse height and V any given pulse height the half width of the distribution η is given by $\eta = (5{\cdot}54\sigma)^{1/2}/\overline{V} = -2{\cdot}36/m\overline{V}$, where σ is the variance of the distribution and $m = y/(\overline{V} - V)$, y being a function which is obtained from tables (Jahnke and Emde 1933), using the experimental values of counts per second for a given pulse height V. In fig. 1 we give the relation between y and V obtained in this manner from 'integral bias curves' by using various luminescent crystals and a homogeneous alpha-particle source (5 Mev) and also by using the neon lamp source. It can be seen that the experimental values confirm the expected linear relation between y and V. The broken horizontal lines in fig. 1 indicate the values of y for 98% (A) and 2% (B) of the total counts per second. Experimental observations outside these limits are not useful for obtaining values of y, as the relative statistical errors become large and are much magnified in the final value of y. Curves 1, 2, and 3 were obtained with thin flat crystals of scheelite, anthracene and naphthalene containing stilbene. Curves 4 and 5 were for crystals with many internal flaws and surface irregularities, while curve 6 was for the neon lamp pulses.

(iii) *Fluctuations in the Photomultiplier*

By using the neon lamp source we eliminate pulse spread due to the photon source and so we can investigate the dependence of pulse distribution on multiplier characteristics.

(*a*) *Effect of multiplier gain.* Using a low intensity steady light source the gain of the multiplier was investigated under 'static' conditions by comparing photocathode and collector electrode currents. It is found that the gain M is given in terms of the overall applied voltage v (equal volts per stage) by

$$M=(v/v_0)^{\gamma}. \qquad \ldots\ldots(4)$$

For the multiplier used $v_0=98{\cdot}2$ volts and $\gamma=5{\cdot}35$ respectively. By replacing the steady source with an anthracene crystal and alpha source the gain was investigated under pulsed conditions. Equation (4) was found to hold provided

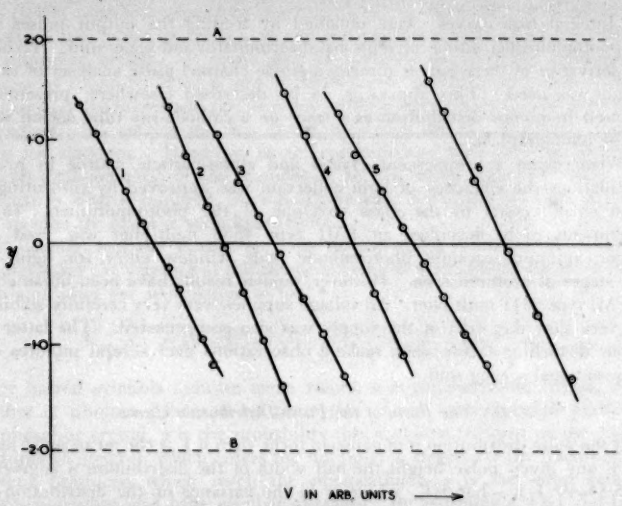

Fig. 1. Variation of the function y of eqn. (8) with scintillation pulse magnitude.
1. Scheelite. 2. Anthracene. 3. Stilbene in naphthalene. 4. Copper activated zinc sulphide. 5. Thallium activated potassium iodide. 6. Neon lamp pulses.

that the interstage capacity was made large enough to avoid voltage changes between dynodes during the transit of a pulse of charge. A value of $\gamma=5{\cdot}34$ was obtained over a range extending to 1 500 volts (150 v/stage). At 1 500 volts the gain was $2{\cdot}2\times10^6$. The dependence of the half width η of the pulse distribution on gain was investigated and was found to be small, as would be expected, since from eqn. (3) $\eta=\eta_0\{s/(s-1)\}^{1/2}$. With the above multiplier constants the measured value of η changes from 0·19 at 700 volts (overall) to about 0·17 at 1 200 volts for the given mean pulse magnitude. From measurement of the effective collector electrode capacity and the overall gain it was deduced that an average of 360 photoelectrons were produced per scintillation. If we assume that all photoelectrons enter the multiplying stages

and also apply the correction factor $\{s/(s-1)\}^{1/2}$ then the half width expected from statistical fluctuations in this number is 0·135. Since the fraction of photoelectrons entering the multiplying stages and the correction factor $\{s/(s-1)\}^{1/2}$ are inter-dependent quantities, the true value of each must be obtained by successive approximations. However, a change from 1·00 to 0·60 in the fraction of photoelectrons collected alters the quantity $\{s/(s-1)\}^{1/2}$ by less than 1% and so only two stages of approximation are required. The average experimental value for the particular conditions was 0·174, which indicates that only about 60% of the photoelectrons enter the multiplying stages.

(*b*) *Effect of incident light pulse intensity.* By using the neon lamp source and neutral filters the dependence of the half width of the pulse distribution on light pulse intensity was determined. Figure 2 shows in a striking pictorial way the appearance of statistical fluctuations as the light pulse intensity is reduced. The

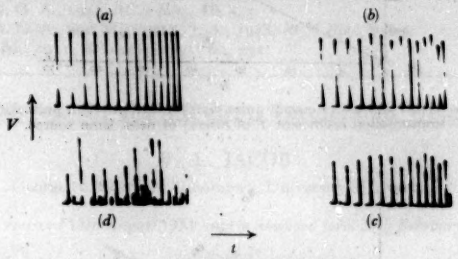

Fig. 2. Multiplier output pulses for different light pulse intensities from neon lamp source. (V is pulse height, t is time.)

(*a*) 20 000 photoelectrons per pulse; $\eta=0{\cdot}015$
(*b*) 2 000 photoelectrons per pulse; $\eta=0{\cdot}047$
(*c*) 200 photoelectrons per pulse; $\eta=0{\cdot}15$
(*d*) 6 photoelectrons per pulse; $\eta=0{\cdot}94$

photographs give the appearance of the multiplier output pulses on a monitor cathode-ray tube for four different intensities. Figure 2 (*a*) shows the uniform pulse height obtained when the number of photoelectrons produced is very large ($\sim 2\times 10^4$) and for which number η is almost zero. For fig. 2 (*d*) the pulse intensity was so small that only about six photoelectrons were produced per pulse, giving a half width of $\eta=0{\cdot}94$. The random thermionic emission pulses, due to single electrons, can be seen among the regularly spaced light pulses in this photograph. Figure 3 shows the linear relation found between η^2 and the inverse mean light pulse intensity, given by the transmission coefficient of the filters which is expected from eqn. (3).

(iv) *Study of Pulse Spread due to the Luminescent Crystal*

Various crystals were used in these investigations, some being optically perfect and others having marked flaws and irregularities. The half width and mean pulse magnitude were measured for standard photomultiplier conditions, using a 5 Mev alpha-particle source as excitor. After each crystal had been studied the neon lamp light pulse source was swung into position over the multiplier cathode and the values of half width and mean pulse magnitude determined. By means of this check any variations in the multiplier behaviour

become apparent. The values obtained for the neon lamp and for various crystals are plotted graphically in fig. 4 to show the relation between η^2 and $1/\overline{V}$. It is seen that all values for the neon lamp and the perfect crystals lie on the same straight line which passes through the origin, that is, pulse spread is mainly determined by the photomultiplier characteristics. However, the points for imperfect crystals deviate considerably from this straight line depending on the degree of imperfection in the crystal. It should be noted that, as would be expected, all imperfect crystals give points lying above the straight line.

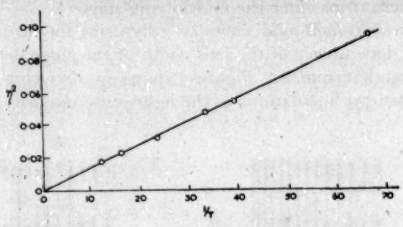

Fig. 3. Variation of half width η of output pulse distribution with light pulse intensity (given by transmission coefficient T of filters) of neon lamp source.

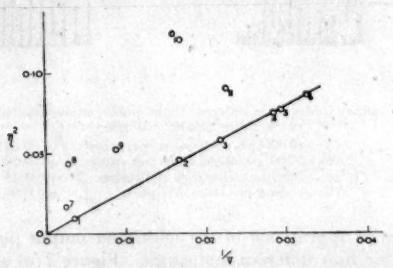

Fig. 4. Variation of half width η of output pulses with mean pulse size $\overline{V}$ for scintillations from various crystals and for neon lamp light pulses.

1. Neon lamp pulses; flawless crystals. 2. Scheelite. 3. 4. Anthracene in naphthalene. 5. Stilbene in naphthalene. 6. Stilbene in naphthalene; crystals with flaws. 7. Thallium activated potassium iodide. 8. Copper activated zinc sulphide. 9. Anthracene. 10. Anthracene in naphthalene. 11. Stilbene.

§ 4. CONCLUSION

The above results are of importance when using the scintillation counter for energy measurements. They indicate which factors are mainly responsible for the spread in pulse magnitude at particle energies in the range 1–10 MEV. These are the number of photoelectrons produced per scintillation and the optical quality of the phosphor crystal together with its intrinsic efficiency for converting particle energy to luminescence. The effects of multiplier dynodes are seen to be relatively small compared with the above factors.

It would seem very desirable to improve the photoelectron collection efficiency for the two types of photomultiplier investigated, and if possible to improve the intrinsic efficiency of phosphors. Since only 20% of the absorbed energy

appears as luminescence a fundamental investigation of the non-radiative processes by which the other 80% is lost would be useful. Some attempts to investigate the latter have been made recently by Schön (1951), by Broser and Warminsky (1951) for inorganic sulphide crystals and by Birks (1950) for anthracene.

ACKNOWLEDGMENT

We wish to thank the Department of Scientific and Industrial Research for a grant to one of us (G. T. W.).

REFERENCES

BIRKS, J. B., 1950, *Proc. Phys. Soc.* A, **63**, 1294.
BROSER, I., and WARMINSKY, R., 1951, *Z. Naturforsch.*, 6a, 85.
ENGSTROM, R. W., 1947, *J. Opt. Soc. Amer.*, **37**, 420.
HOYT, R., 1949, *Rev. Sci. Instrum.*, **20**, 178.
JAHNKE, E., and EMDE, F., 1933, Tables of Functions (Leipzig : Teubner).
MORTON, G. A., 1949, *RCA Rev.*, **10**, 523.
MORTON, G. A., and MITCHELL, J. A., 1948, *RCA Rev.*, **9**, 632.
SCHÖN, M., 1951, *Z. Naturforsch.*, **6a**, 251.

The Current in the Electron Immersion Objective

BY L. JACOB

George Holt Physics Laboratory, University of Liverpool

MS. received 13*th August* 1951, *and in amended form* 20*th February* 1952

ABSTRACT. It is shown that for an electron immersion objective under the condition of constant cut-off voltage the emission current is uniquely defined by the cross-over potential. There is thus some theoretical foundation for the empirically observed law that the current at zero modulation voltage depends only on the three-halves power of the cut-off voltage.

§1. INTRODUCTION

IT is well known that the electron immersion objective, in common with all other electronic devices which work under space charge limited conditions, obeys the three-halves power law. The theoretical problem, however, of determining the importance of the various parameters, in connection with any desired modulation characteristic, is somewhat complicated. A contributing feature is the special geometrical construction, which is necessary in order to provide a rotationally symmetrical beam, of the current density required for practical operations. The main difficulty arises from the large values of the ratio of aperture diameter to cathode–aperture separation. This may be as high as 20 to 1, and thus emphasizes the 'hole' effect. For this reason it has been customary to base design data mainly on empirical results; these usually cover a large number of variations carried out on model systems, either in demountable tubes or in separate processed units. In this way it was found that for systems with different geometry but with a common cut-off voltage V_{c0} the current furnished by the system was approximately constant and depended only on the value of the cut-off voltage.

Examination of the modulation characteristic revealed an empirical law of the form $I = KV^{7/2}/V^{2}_{c0}$ for the current at any voltage V, up from the cut-off point V_{c0},

where the constant K has a value of about 3 ; this law appears valid to several per cent over a considerable portion of the curve. When $V = V_{co}$ then $I = KV_{co}^{3/2}$, which is the well-known three-halves power relation, for the cut-off voltage is directly proportional to the anode voltage. The purpose of the present paper is to seek an explanation for the constant value of current determined by a constant value of cut-off voltage. Different geometries were tried in which the cathode to modulator spacing was varied over a range of 10 to 1, keeping anode spacing, modulator aperture and thickness constant. The system is shown in the figure.

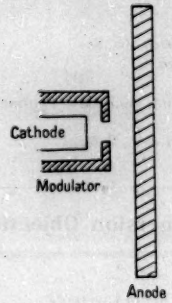

Cathode 1·8 mm diameter.
Modulator to anode 1 mm.
Cathode/modulator spacing—variable.
Modulator aperture 1·0 mm.
,, diameter 10 mm.
,, thickness 0·3 mm.

§2. SOME CROSS-OVER PROPERTIES

It was shown earlier (Jacob 1950a) that the axial potential distribution of the immersion system can be expressed as a sum of exponential terms involving certain constants of the system. Over the ranges explored this can be approximately represented by the simple law $V = Ae^{kz}$, where A is a voltage scale factor connected with the form of the field, that is, it depends separately on anode voltage and modulator bias, while k depends on the geometry. On applying this to an analysis of the trajectory equation it was possible to derive certain properties of the cross-over (Jacob 1950 b). These may be summarized as follows :

Distance of cathode to cross-over	$=8\pi/3k\sqrt{3}$	.....(1)
Potential at cross-over	$=A\exp(8\pi/3\sqrt{3})$	.....(2)
Radius of cross-over	$=(2\tan\theta/k)\exp(-2\pi/3\sqrt{3})$	.....(3)

where θ is the limiting angle of emission, within the paraxial range, of electrons leaving the centre of the cathode. This is taken to have a constant value throughout the analysis.

It may thus be seen that the potential at the cross-over simply depends on the value of the constant A. This can be derived from the plots in the electrolytic tank for any set of field conditions. A typical set of values is given in table 1 for a range of variation in cathode to modulator, C/M, spacing of 10/1.

Table 1

Modulator thickness 0·2 mm; modulator aperture diameter 1·0 mm; separation from anode 1 mm.

C/M (mm).	0·05	0·10	0·30	0·50
A (for 30 v cut-off at zero bias).	0·96	0·98	1·15	0·72

These observations indicate a tendency for the potential at the cross-over to remain constant over a substantial variation in spacing, provided the condition of constant cut-off voltage is maintained for each geometry.

The variation for the larger spacings can be accounted for by an error of some 10% in determining the cut-off voltage under the conditions in the tank, since the voltage scale had to be stepped down by a factor of 12.

Independent confirmation of the constancy of the cross-over potential was obtained by actual ray tracing on a similar type of objective whose field plots were also determined in the tank (Einstein and Jacob 1948) for each variation in geometry.

The actual position and size of the cross-over will, of course, vary from geometry to geometry, depending as it does on the k of the system according to (1) and (3); however, the gradient at the cross-over (which is numerically k times its value of potential) does not vary greatly except for the closest spacing for which k has its highest value. As the potential at the cross-over is directly proportional to the potential on the anode, which in turn governs the cut-off voltage, we see that the cross-over voltage and cut-off voltage are proportional. The approximate relationship between anode and cut-off voltage can sometimes be calculated in simple cases, e.g. where the anode and cathode are the end pieces of a flat pill box at potentials V_2 and V_1 respectively, spaced infinitely close to, but insulated from, the body which forms the modulating electrode kept at zero potential. The potential V at any point (z, r) is given (Jacob 1951) in terms of the radius a and length $2l$ of the cylinder by

$$V=(V_1+V_2)\left[\frac{J_0(k_1r)\cosh k_1z}{k_1aJ_1(k_1a)\cosh k_1l}+\frac{J_0(k_2r)\cosh k_2z}{k_2aJ_1(k_2a)\cosh k_2l}+\dots\right]$$
$$+(V_2-V_1)\left[\frac{J_0(k_1r)\sinh k_1z}{k_1aJ_1(k_1a)\sinh k_1l}+\frac{J_0(k_2r)\sinh k_2z}{k_2aJ_1(k_2a)\cosh k_2l}+\dots\right] \qquad \dots\dots(4)$$

where J_0 and J_1 represent Bessel functions of zero and first order respectively, and k_1, k_2 etc. are constants defined by the roots of the function. For points on the axis $J_0(k_nr)=1$, hence the axial gradient at the cathode can be derived by differentiation of (4) with respect to z. The cut-off condition corresponds to zero gradient at the centre of the cathode, apart from initial velocity effects, i.e. the neutralization of the field which penetrates through from the anode, by the field from the modulator. In this case the zero equipotential just meets a central region of the emitting cathode, while the gradient over the remainder of the surface is negative.

The relation between the cut-off and anode voltages for any system of such simple geometry is then given by

$$\frac{V_1+V_2}{V_2-V_1}=-\frac{\Sigma(\coth k_nl)/J_1(k_na)}{\Sigma(\tanh k_nl)/J_1(k_na)}. \qquad \dots\dots(5)$$

If V_1 is desired to have any value (in this case positive, and numerically equal to the cut-off value) the corresponding anode voltage V_2 can be found in terms of the geometrical factors (a, l), but these would require to be worked out for each geometry.

§3. THE CURRENT IN THE BEAM

In the following analysis it is assumed that the static distribution is not affected by the space charge, and the complicating factor of initial velocities is

neglected. We make use of the following well-known approximation for rotationally symmetrical fields:

$$V_{(z,r)} = V_z - \frac{r^2}{4} V_z'' + \frac{r^4}{64} V_z^{iv} \ldots \qquad \ldots\ldots(6)$$

and apply four fundamental conditions for space charge flow: (*a*) Poisson's equation, (*b*) current density = space charge density × velocity, (*c*) $v = (2eV/m)^{1/2}$ and (*d*) use of relation $V = Ae^{kz}$. Take any element of space within the region of current flow, then

$$\frac{1}{r}\frac{\partial}{\partial r}\left(r\frac{\partial V}{\partial r}\right) + \frac{\partial^2 V}{\partial z^2} = -4\pi\rho \qquad \ldots\ldots(7)$$

giving

$$-V_s'' + \tfrac{1}{4}r^2 V_z^{iv} + V_s'' = -4\pi\rho \qquad \ldots\ldots(8)$$

and

$$\rho \simeq (-r^2 k^4 V_s)/16\pi \qquad \ldots\ldots(9)$$

This gives the volume density of charge at a point distant r from the axis in terms of the potential on the axis and the k of the system. Now from (*b*)

$$j = \rho\left\{\frac{2e}{m}(V_s - \tfrac{1}{4}r^2k^2V_s)\right\}^{1/2} = \left\{\frac{r^2k^4}{16\pi}\left(\frac{2e}{m}\right)^{1/2}(1-\tfrac{1}{4}r^2k^2)^{1/2}\right\}V_s^{3/2}. \qquad \ldots\ldots(10)$$

This is the current passing through unit area at the point (z, r). Now imagine a ring element of width dr to embrace this point:

Current in ring element $j_r = (2\pi r^3 k^4/16\pi)(2e/m)^{1/2}(1-\tfrac{1}{4}r^2k^2)^{1/2} V_s^{3/2}\, dr$,

Current across section of beam $j_s = \tfrac{1}{8}(2e/m)^{1/2} V_s^{3/2} \int_0^R r^3 k^4 (1-\tfrac{1}{4}r^2k^2)^{1/2}\, dr$,

where the limit of r corresponds to the periphery of the beam.

$$j_s \simeq C_1 V_s^{3/2} \int_0^R r^3 k^4 (1 - r^2k^2/8)\, dr \text{ since } r \ll k$$
$$\simeq C_1 V_s^{3/2}\left[\tfrac{1}{4}r^4k^4 - \tfrac{1}{48}r^6k^6\right]_0^R.$$

Now, it is clear that V_s can be taken anywhere along the beam axis, e.g. at the cross-over. In this case the limits of R correspond with the radius at this point, i.e. $C_2 \tan\theta/k$, where C_2 is a numerical constant given in (3). Then current over section at cross-over

$$\simeq C_1 V_{cr}^{3/2}\left[\frac{C_2^4 \tan^4\theta}{4} - \frac{C_2^6 \tan^6\theta}{48}\right].$$

As C_1, C_2, θ are constants on the simple theory, it is seen that the current in the beam depends primarily on the potential at the cross-over; hence, for different systems which have the same value of cut-off potential, and hence of cross-over potential, the current should have a unique value over this range of geometries. This is found in practice.

This relation should also hold when the beam is modulated. In this case it is necessary to determine the value of A corresponding to each modulation point. A typical set of values is given in table 2 (obtained from the tank plots) where M is the modulator voltage.

Table 2

M	0	−0·54	−1·0	−1·5
A	0·43	0·30	0·21	0·04

There is, however, some uncertainty in the value of θ when the modulation is applied because its effect is to decrease both the emitting area and the beam angle, and it is not clear as to how θ varies with modulation. This means that it is not yet possible to predict with any accuracy the theoretical shape of the full modulation curve.

REFERENCES

EINSTEIN, P. A., and JACOB, L., 1948, *Phil. Mag.*, **39**, 20.
JACOB, L., 1950 a, *Proc. Phys. Soc.* B, **63**, 75 ; 1950 b, *J. Appl. Phys.*, **21**, 966 ; 1951, *Introduction to Electron Optics* (London : Methuen).

An Improved Method for Measurements of Optical Constants by Reflection

BY D. G. AVERY
Royal Holloway College, University of London*

Communicated by S. Tolansky; MS. received 3rd January 1952

ABSTRACT. At wavelengths outside the photographic range the determination of the optical constants of absorbing media involves the measurement of intensity changes on reflection at the surface of the medium. A review of previous methods for their determination is made and the experimental difficulties are indicated. A method is described which surmounts some of these difficulties by avoiding the direct measurement of reflection coefficients. The accuracy to be expected from the method and an example of its use are briefly discussed.

§1. REFLECTION METHODS—GENERAL THEORY

THE determination of refractive index n and absorption index k from measurements on reflected intensities has been described in general terms by Tousey (1939). In principle the method consists in measuring some characteristic of the reflection at various angles of incidence. Then, if the measured values of the characteristic at angles of incidence θ_1, θ_2, etc., for plane polarized light of azimuth ϕ, be R_1, R_2 . . . . etc., we have $R_1 = F(n, k, \theta_1, \phi)$, $R_2 = F(n, k, \theta_2, \phi)$, etc., where the function F is obtained from the appropriate Fresnel's equation for the reflection. Then the pair of values of n and k which can be obtained from the simultaneous solution of these equations are the optical constants of the medium. Since the algebraic relations cannot be solved directly for n and k the equations are solved graphically.

§2. THE MEASUREMENT OF REFLECTION COEFFICIENTS

Of the various characteristics of a given reflection, the one most generally chosen for measurement is the simple 'reflection coefficient', i.e. the relative intensity after reflection under given conditions of incidence and polarization. This method was described by Collins and Bock (1943) and has recently been discussed in detail by Simon (1951), who publishes some graphs relating the reflection coefficient to n and k for angles of incidence 20° and 70°. The measurement of reflection coefficients, particularly at non-normal incidence, presents a number of difficulties which will be briefly discussed below.

* Now at Telecommunications Research Establishment, Great Malvern, Worcs.

Perhaps the greatest of these problems are those associated with the large decrease in effective aperture of the reflecting surface as the angle of incidence is increased. As in many cases where the optical constants of single crystals, etc., are being determined, the specimens available tend to be rather small, and since in no case must the specimen itself become the limiting aperture of the optical system, it follows that the beam cross section used must be very small, with consequent loss in intensity if beams of only small divergence are to be employed. This problem becomes particularly acute when the values of n and k are such that, to maintain the accuracy of the experiment, one reflection coefficient measurement must be made at 70°, or even higher, incidence.

A second difficulty is that, for accurate reflection coefficient measurements, not only must the beams used have a constant intensity over their cross sections, but also the same portion of the photosensitive surface of the detector must be used at all angles, to avoid errors due to variation in photosensitivity across the detector surface. For accurate work (Kuhn and Wilson 1950) this involves the use of diffusing screens in front of both source and detector, with consequent further loss in intensity.

Finally, it is necessary to arrange for the source intensity and detector equipment to be constant over the times (at least several minutes) required to make measurements on a specimen at a given wavelength at, say, three angles of incidence and, in addition, to obtain a reading for the incident intensity or for the reflection from a reference mirror.

§3. THE METHOD ADOPTED

Most of these difficulties no longer exist if, instead of taking as the reflection characteristic the reflection coefficient for a given plane of polarization, one measures the ratio of the reflection coefficients for incident light polarized in and perpendicular to the plane of incidence. The basic requirements of the optical system in this case are then simply (*a*) the polarizer must be such that the beam passing through it suffers no lateral shift on rotating the plane of polarization, and (*b*) if the light incident on the polarizer has not equal components in the two planes of polarization the ratio of the components must be known.

If these conditions are satisfied, then even if the specimen is so small, or irregular in shape, that it becomes the limiting aperture at high angles of incidence, this introduces no errors since the aperture is the same for both planes of polarization. Motion of the reflected image over the detector surface as the incidence angle varies is of no importance since no absolute measurements of reflection coefficient need be made. Furthermore, the period of time for which the source and detector need be stable is only the time necessary to turn the polarizer through 90° and to take two meter readings. In addition, no absolute measurements of incident intensity are required.

The formulae relating the ratio of the reflection coefficients of a substance for two planes of polarization to the optical constants can be derived from Fresnel's equations. If the complex refractive index of the substance be $N=n(1-ik)$, defined above, and if the ratio of the reflection coefficients be ρ^2, then at angle of incidence θ

$$\rho^2=\frac{a^2+b^2-2a\sin\theta\tan\theta+\sin^2\theta\tan^2\theta}{a^2+b^2+2a\sin\theta\tan\theta+\sin^2\theta\tan^2\theta},$$

where $N^2-\sin^2\theta=(a-ib)^2$.

Curves relating ρ^2 to n and k for angles of incidence of 30°, 45°, 60°, 73° and 80° have been plotted from computations for values of n between 2·0 and 8·0 and values of k between 0 and 2·0. The curves for 60° and 80° incidence are shown in figs. 1 and 2. From two or more measured values of ρ^2 at different angles of incidence, tables of values of n and k can be drawn up from these graphs and plotted against n and k as axes. In order to obtain well-defined intersections it is desirable to arrange the angles of incidence so that measurements of ρ^2 are made on both sides of the quasi-polarizing angle for the material. One such intersection for three measured values of ρ^2 is shown in fig. 3.

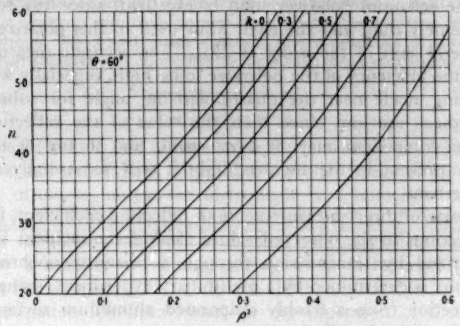

Fig. 1. Curves relating ρ^2 to n and k for 60° incidence.

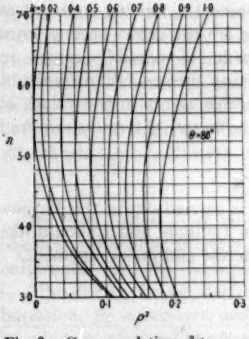

Fig. 2. Curves relating ρ^2 to n and k for 80° incidence.

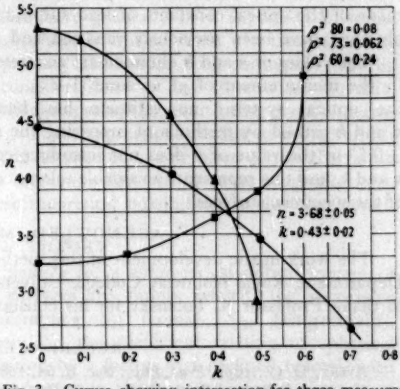

Fig. 3. Curves showing intersection for three measured values of ρ^2 plotted against n and k as axes.

§ 4. TECHNIQUE, AND THE ERRORS ARISING IN THE METHOD

The specimen is fastened to an adjustable mount at the centre of a hollow block whose temperature can be varied with coolants, etc. This block is mounted on a shaft with a slow-motion drive and a vernier scale to measure angles of incidence to 1′ of arc. The detector is mounted on an arm rotating about the

same axis as the main shaft, and geared to it with a 2 : 1 ratio, so that, once adjusted, the reflected beam remains on the detector as the angle of incidence is varied. The whole is provided with a vacuum chamber for work with cooled specimens.

Measurements are at present being made at wavelengths in the infra-red, and the polarizer employed is a pile of selenium films, constructed and used as described by Elliott, Ambrose and Temple (1948).

The principal source of error in these measurements lies in the possible non-fulfilment of condition (*a*) referred to above, that is, in possible movement of the reflected beam over the detector surface as the polarizer is rotated. In this connection the selenium polarizer used is excellent, since the selenium films used are extremely thin, and the eight films used in this polarizer would only produce a lateral shift of the order of 25μ. For accurate measurements it is necessary for the efficiency of the polarizer to be high, especially when measurements are being made near the quasi-polarizing angle for substances whose absorption indices are low, since then the value of the reflection coefficient for the parallel component may be very small, and if any of the unwanted component is present in the incident light it will be strongly reflected and cause serious errors.

As in the case of direct measurements of reflection coefficient, it is necessary to make corrections to the observed values of ρ^2 if the incident light has been partially polarized by transmission through a prism monochromator. This correction factor is determined by a preliminary experiment, using near-normal incidence reflection from a freshly evaporated aluminium surface, conditions under which the real value of ρ^2 is unity.

With the system as described, some preliminary measurements have been made of the optical constants of lead sulphide and lead telluride. The values obtained have been previously reported and discussed (Avery 1951).

The values of n and k obtained are accurate to some 4%, arising from errors in the measurement of ρ^2 of some 1–2%. These are the errors arising from the optical system: no estimate has been made of possible errors in n and k caused by methods of preparing the reflecting surface. A tolerance of $\pm 0{\cdot}5^\circ$ in the value of θ does not introduce comparable errors in the values of n and k, and this represents a valuable tolerance in the degree of flatness required of the specimen surfaces.

ACKNOWLEDGMENTS

The work in the development of this method was carried out in the Physics Department, Royal Holloway College, University of London, and I should like to thank Professor S. Tolansky for his constant interest and encouragement.

REFERENCES

Avery, D. G., 1951, *Proc. Phys. Soc.* B, **64**, 1087.
Collins, J. R., and Bock, R. O., 1943, *Rev. Sci. Instrum.*, **14**, 135.
Elliott, A., Ambrose, E. J., and Temple, R., 1948, *J. Opt. Soc. Amer.*, **38**, 212.
Kuhn, H., and Wilson, B. A., 1950, *Proc. Phys. Soc.* B, **63**, 745.
Simon, I., 1951, *J. Opt. Soc. Amer.*, **41**, 336.
Tousey, R., 1939, *J. Opt. Soc. Amer.*, **29**, 235.

Primary Aberrations and Conjugate Change

By C. G. WYNNE
Wray (Optical Works) Ltd., Bromley, Kent

MS. received 17*th December* 1951

ABSTRACT. Expressions are derived, in terms of the functions normally used in optical designing, for the variation with conjugates of the primary aberrations of any symmetrical system with isotropic object and image spaces. The possibilities of invariance of the aberrations, or their simultaneous correction for more than one magnification, are discussed.

§ 1. INTRODUCTION

THE proposition that "it is impossible, by means of any combinations of reflexions and refractions, to produce a *perfect* image of an object at two different distances, unless the instrument be a telescope" was given by Clerk Maxwell in 1858, and since that time various aspects of the laws governing the variations of aberrations with changes of magnification have been investigated by a number of writers, among them Herzberger (1931, 1946), Boegehold and Herzberger (1935), T. Smith (1948) and Grenat (1949). In most cases the investigation has been based on the expansion of the Hamiltonian characteristic function or Bruns' eikonal, the mathematics not always being simple, and where analytic expressions for the variation of the primary aberrations have been deduced these have generally been expressed in terms of special functions not normally calculated in optical work. In this paper it is shown that the variations of the primary aberrations with conjugates may be deduced from extremely simple considerations for any systems having axial symmetry and isotropic object and image spaces, the result being given in terms of the normal aberration functions. These expressions readily give the various possibilities of, and conditions for, invariance of one or more of the aberration coefficients, or their simultaneous correction for two or more magnifications, and the physical realization of these theoretical possibilities is also considered.

§ 2. THEORY

The first order aberration coefficients for a symmetrical optical system of spherical reflecting or refracting surfaces are simply related, the successive coefficients for the oblique aberrations S_{II} (coma), S_{III} (astigmatism), S_V (distortion), being derived from S_I, the coefficient relating to spherical aberration, by successive multiplication by a factor $\bar{A}/A$ (defined below), with the addition of the Petzval field curvature in the last case; for an aspherical surface, the additional oblique aberrations are similarly formed by successive multiplication of the axial aberration term by a factor HE. The total first-order aberration of the system is the sum of these surface coefficients. Longhurst (1950) has shown that the coefficients relating to spherical aberration of principal rays for a system of spherical surfaces may be expressed in a form representing an addition to the above series, and by an obvious extension the corresponding coefficient for aspheric surfaces, denoted below by S_{VI}, may be similarly

included. This coefficient is contained in the expansion of the eikonal given by Schwarzschild (1905), but is disregarded by him in his discussion of the primary aberrations. Using a notation similar to that given by Hopkins (1950), the first-order aberration coefficients for a single surface may be written

$$\left.\begin{aligned} &S_{\mathrm{I}} = A^2 y \Delta(u/n) + 8ay^4\Delta(n) = \sigma_{\mathrm{s}} + \sigma_{\mathrm{a}} \\ &S_{\mathrm{II}} = \sigma_{\mathrm{s}} \frac{\bar{A}}{A} + \sigma_{\mathrm{a}} HE, \qquad S_{\mathrm{V}} = \sigma_{\mathrm{s}} \left(\frac{\bar{A}}{A}\right)^3 + PH^2 \frac{\bar{A}}{A} + \sigma_{\mathrm{a}} (HE)^3 \\ &S_{\mathrm{III}} = \sigma_{\mathrm{s}} \left(\frac{\bar{A}}{A}\right)^2 + \sigma_{\mathrm{a}} (HE)^2, \qquad S_{\mathrm{VI}} = HE(S_{\mathrm{V}} + PH\bar{A}\bar{y}) \end{aligned}\right\} \quad \ldots\ldots(1)$$

where y is the intersection height on the surface for a paraxial ray at the conjugates considered, u its angle with the lens axis, i its angle of incidence, n the refractive index, P the Petzval field curvature, H the Smith–Helmholtz invariant, Δ denotes the change on refraction, $A = ni$, a is the coefficient of fourth power asphericity, given by $x = ay^4$, where x is the departure of the surface from sphericity; a bar over any symbol indicates that it relates to a paraxial principal ray through the stop centre instead of to the paraxial ray from the object.

Again following Hopkins (1950), $\bar{A}/A = n\bar{i}/ni = H(E + 1/Ay)$ and $HE = \bar{y}/y$, the quantity E so defined being generally derived in practice from data of a paraxial ray from the object, using Seidel's difference formula.

Clearly the aberrations of pupil imagery, for which the object plane (field stop) is the effective stop, can be expressed by equations identical with (1), with those quantities relating to ray positions with and without bars interchanged, n, a, and P remaining the same in each case; and by definition $\overline{HE} = 1/HE$, $H = -\bar{H}$. Denoting these first-order aberration coefficients of pupil imagery by $\overline{S_{\mathrm{I}}}$, $\overline{S_{\mathrm{II}}}$, etc., then by definition $\overline{S_{\mathrm{I}}} = S_{\mathrm{VI}}$, $\overline{S_{\mathrm{VI}}} = S_{\mathrm{I}}$, and by simple algebra it may be shown that

$$\overline{S_{\mathrm{V}}} - S_{\mathrm{II}} = H\Delta(u^2), \quad \overline{S_{\mathrm{III}}} - S_{\mathrm{III}} = H\Delta(u\bar{u}), \quad \overline{S_{\mathrm{II}}} - S_{\mathrm{V}} = H\Delta(\bar{u}^2). \quad \ldots\ldots(2)$$

For example, from eqns. (1)

$$S_{\mathrm{VI}} = \overline{S_{\mathrm{I}}} = HE(S_{\mathrm{V}} + PH\bar{A}\bar{y}),$$

and since $$\overline{S_{\mathrm{II}}} = \overline{S_{\mathrm{I}}}\bar{H}\bar{E} + \bar{H}\bar{A}\Delta(\bar{u}/n)$$

and $$\overline{S_{\mathrm{I}}} = \bar{A}^2\bar{y}\Delta(\bar{u}/n) + 8a\bar{y}^4\Delta(n),$$

$$S_{\mathrm{V}} = \overline{S_{\mathrm{II}}} + \bar{A}\bar{H}\{P\bar{y} - \Delta(\bar{u}/n)\}$$

$$S_{\mathrm{V}} - \overline{S_{\mathrm{II}}} = \bar{H}\Delta\left[n\bar{i}\left(-\frac{\bar{\alpha}}{n} - \frac{\bar{u}}{n}\right)\right] = -H\Delta(\bar{u}^2 - \bar{\alpha}^2) = -H\Delta\bar{u}^2,$$

and similarly in the other cases.

On summing through the complete system the intermediate terms on the right-hand side of each of eqns. (2) cancel, giving

$$\left.\begin{aligned} &\Sigma\overline{S_{\mathrm{V}}} - \Sigma S_{\mathrm{II}} = H(u_{\lambda}'^2 - u_1^2) \\ &\Sigma\overline{S_{\mathrm{III}}} - \Sigma S_{\mathrm{III}} = H(u_{\lambda}'\bar{u}_{\lambda}' - u_1\bar{u}_1) \\ &\Sigma\overline{S_{\mathrm{II}}} - \Sigma S_{\mathrm{V}} = H(\bar{u}_{\lambda}'^2 - \bar{u}_1^2), \end{aligned}\right\} \quad \ldots\ldots(3)$$

where u, u_{λ}', $\bar{u}$, $\bar{u}_{\lambda}'$, are the angles with the axis of the paraxial ray and paraxial principal ray in the object and image spaces. These equations have applications

in other connections than the present one; thus the third equation shows how the coma of stop imagery $\overline{S_{II}}$, which is of importance in considerations of the intensity of illumination in oblique imagery (Slussareff 1941), depends only on the primary image distortion, the angle of field and the pupil magnification.

Now the change in the primary aberration coefficients produced by change of stop position is very simply expressed, since the effect is to add to HE, in eqns. (1), a term constant throughout the system. A change of stop position for pupil imagery is equivalent to a change of object position, so that, by applying eqns. (2) to the equations showing the variation of $\overline{S_{II}}$, $\overline{S_{III}}$ and S_V with object position, the changes of S_{II}, S_{III} and S_V with conjugates are readily derived. If the object be considered to be moved such a distance as to add a term $\overline{H\delta E}$ to $\overline{HE}$ in the expression for $\overline{S_{II}}$, $\overline{S_{III}}$ and $\overline{S_V}$, then, from the equations for these coefficients analogous to eqns. (1), the new values $\overline{S_{II}}^*$, $\overline{S_{III}}^*$, etc., are given, after some reduction, by

$$\left.\begin{aligned}
\Sigma\overline{S_{II}}^* &= \Sigma\overline{S_{II}} + \overline{H}\delta\overline{E}\,\Sigma\overline{S_I}\\
\Sigma\overline{S_{III}}^* &= \Sigma\overline{S_{III}} + 2\overline{H}\delta\overline{E}\,\Sigma\overline{S_{II}} + (\overline{H}\delta\overline{E})^2\Sigma\overline{S_I}\\
\Sigma\overline{S_V}^* &= \Sigma\overline{S_V} + \overline{H}\delta\overline{E}\,\Sigma(3\overline{S_{III}} + PH^2) + (\overline{H}\delta\overline{E})^2\Sigma 3\overline{S_{II}} + (\overline{H}\delta\overline{E})^3\Sigma\overline{S_I}\\
\Sigma\overline{S_{VI}}^* &= \Sigma\overline{S_{VI}} + \overline{H}\delta\overline{E}\,\Sigma(3S_{II} + \overline{S_V}) + (\overline{H}\delta\overline{E})^2\Sigma(3S_{III} + 3\overline{S_{III}} + 2PH^2)\\
&\quad + (\overline{H}\delta\overline{E})^3\Sigma(S_V + 3\overline{S_{II}}) + (\overline{H}\delta\overline{E})^4\Sigma\overline{S_I}.
\end{aligned}\right\} \quad \ldots\ldots(4)$$

Equations equivalent to these have been given by a number of writers; they are given in this form for an aspheric system by Wynne (1949).

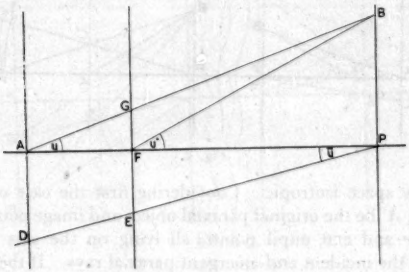

Fig. 1.

If A (fig. 1) be the axial object point for the original imagery, and P the pupil point in the object space, the paraxial ray from A, AB, making an angle u with the axis, and the paraxial principal ray DP making an angle $\bar{u}$ with the axis, then if the object plane be moved to F, the plane through F normal to the axis intersecting AB in G and DP in E, the angle BFP will then be u^*, and the value of $\overline{H\delta E}$ corresponding to this change of conjugates (keeping H constant, i.e. for a constant pupil size and field angle) is given, by definition, to the order of approximation required, by

$$\overline{H}\delta\overline{E} = \mathrm{GF}/\mathrm{FE} = (u^* - u)/\bar{u}. \qquad \ldots\ldots(5)$$

Substituting S_{II}, S_{III} and S_V from eqns. (2) for $\overline{S_V}$, $\overline{S_{III}}$ and $\overline{S_{II}}$, and u^* from eqn. (5) in eqns. (4), the change of the first-order aberrations for a change of conjugates are given by

$$\left.\begin{aligned}
\Sigma S_V^* - \Sigma S_V &= \overline{H}\delta\overline{E}\Sigma\overline{S_I}\\
\Sigma S_{III}^* - \Sigma S_{III} &= \overline{H}\delta\overline{E}\Sigma(S_V+\overline{S_{II}})+(\overline{H}\delta\overline{E})^2\Sigma\overline{S_I}\\
&= \overline{H}\delta\overline{E}\Sigma(2S_V+H\Delta\bar{u}^2)+(\overline{H}\delta\overline{E})^2\Sigma\overline{S_I}\\
\Sigma S_{II}^* - \Sigma S_{II} &= \overline{H}\delta\overline{E}\Sigma(2S_{III}+\overline{S_{III}}+PH^2)+(\overline{H}\delta\overline{E})^2\Sigma(S_V+2\overline{S_{II}})\\
&\quad+(\overline{H}\delta\overline{E})^3\Sigma\overline{S_I}\\
&= \overline{H}\delta\overline{E}\Sigma(3S_{III}+PH^2+H\Delta u\bar{u})\\
&\quad+(\overline{H}\delta\overline{E})^2\Sigma(3S_V+2H\Delta\bar{u}^2)+(\overline{H}\delta\overline{E})^3\Sigma\overline{S_I}\\
\Sigma S_I^* - \Sigma S_I &= \overline{H}\delta\overline{E}\Sigma(3S_{II}+\overline{S_V})+(\overline{H}\delta\overline{E})^2\Sigma(3S_{III}+3\overline{S_{III}}+2PH^2)\\
&\quad+(\overline{H}\delta\overline{E})^3\Sigma(S_V+3\overline{S_{II}})+(\overline{H}\delta\overline{E})^4\Sigma\overline{S_I}\\
&= \overline{H}\delta\overline{E}\Sigma(4S_{II}+H\Delta u^2)\\
&\quad+(\overline{H}\delta\overline{E})^2\Sigma(6S_{III}+2PH^2+3H\Delta u\bar{u})\\
&\quad+(\overline{H}\delta\overline{E})^3\Sigma(4S_V+3H\Delta\bar{u}^2)+(\overline{H}\delta\overline{E})^4\Sigma\overline{S_I}.
\end{aligned}\right\}\quad\ldots\ldots(6)$$

The proof of eqns. (3) and (6) given above is valid for any symmetrical optical system of refracting or reflecting surfaces. The same equations may be shown to be generally valid for any symmetrical imaging system having the

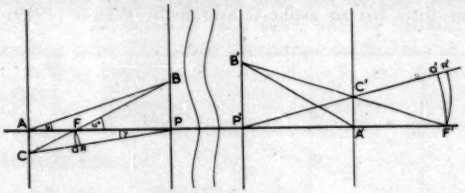

Fig. 2.

object and image space isotropic. Considering first the case of axial spherical aberration, let A, A′ be the original paraxial object and image points and P, P′ the paraxial entrance and exit pupil points, all lying on the axis APP′A′ (fig. 2), and AB, B′A′ be the incident and emergent paraxial rays. If the axial aberration is required of a point F, whose paraxial image is F′, then drawing BF to meet the plane normal to the axis through A in C and taking circles through F, centred on P and C, to intersect CP in Q and R and similarly in the image space; denoting optical path lengths by square brackets, and the aberration associated with the imagery of the point A by ω_A and similarly for the other points, then the aberration required, ω_F is given by

$$\omega_F = -[FB\ldots B'F']+[FP\ldots P'F'] \text{ and } \omega_C = -[FB\ldots B'F']+[RP\ldots P'R'],$$

$$\omega_P = -[QP\ldots P'Q']+[FP\ldots P'F']$$

or
$$\omega_F = \omega_C+\omega_P-\Delta n(QR). \qquad \ldots\ldots(7)$$

If now the first-order values be substituted in eqn. (7), the aberrations for the plane AC being assumed known for a field angle $\bar{u}$, then if the angle APC $=\gamma$,

and again following Hopkins' formulation for the first-order aberrations of a symmetrical system of spherical surfaces, which is also the form of first-order aberration for any symmetrical system,

$$\omega_P = \tfrac{1}{8}\Sigma\overline{S}_I(\gamma/\bar{u})^4$$
$$\omega_C = \Sigma[\tfrac{1}{8}S_I + \tfrac{1}{2}S_{II}\gamma/\bar{u} + \tfrac{1}{4}(3S_{III} + PH^2)(\gamma/\bar{u})^2 + \tfrac{1}{2}S_V(\gamma/\bar{u})^3].$$

From fig. 2, if the angle $BFP = u^*$, $QR = AF \sec u^* + FP - AP \sec \gamma$. From the geometry of the figure, $FP \tan u^* = AP \tan u$, $AF \tan u^* = AP \tan \gamma$. If H be the Smith–Helmholtz invariant for the initial aperture angle u and field angle $\bar{u}$, then $nAPu\gamma = H\gamma/\bar{u}$, the corresponding function for the field angle γ, is also invariant. Substituting in the equation for QR and expanding the trigonometrical functions, to the order of approximation required,

$$-\Delta n\,QR = \tfrac{1}{8}H\frac{\gamma}{\bar{u}}\left[u^2 + 3\frac{\gamma}{\bar{u}}u\bar{u} + 3\left(\frac{\gamma}{\bar{u}}\right)^2\bar{u}^2\right].$$

Substitution in eqn. (7) then gives

$$\left.\begin{aligned}\Sigma S_I^* = \Sigma S_I + (\gamma/\bar{u})\,\Sigma[4S_{II} + \Delta\bar{u}^2] + (\gamma/\bar{u})^2\,\Sigma[6S_{III} + 2PH^2 + 3H\Delta u\bar{u}] \\ + (\gamma/\bar{u})^3\,\Sigma[4S_V + 3H\Delta\bar{u}^2] + (\gamma/\bar{u})^4\,\Sigma\overline{S}_I.\end{aligned}\right\} \ldots\ldots(8)$$

This latter equation is identical with the last of eqns. (6) since $\overline{H}\delta\overline{E} = \gamma/\bar{u}$. Alternatively, the aberration of the point P could be expressed in terms of ω_B and ω_A, instead of ω_C and ω_P, an equation analogous to (7) resulting. By

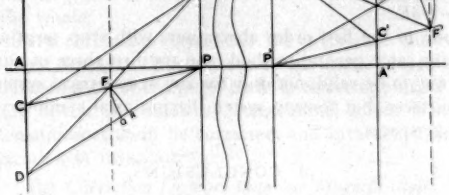

Fig. 3.

inserting the first-order aberrations in this case, and equating coefficients in this and eqn. (8), the relationships between S_{II} and $\overline{S_V}$ etc. given in eqns. (2) are obtained, so that these too are valid for any symmetrical system having isotropic object and image spaces.

The first-order oblique aberrations for a second pair of conjugates in terms of those of the first is given by a similar procedure. The simpler case of aberrations in a meridian plane will be considered here, though the same method is obviously applicable to the general case. Let C, C′ in fig. 3 be paraxial object and image points on the initial conjugate planes PP′, BB′, the paraxial pupil centres and edges, respectively, and let F, lying on the line CP, be a point on a new object plane; then joining FB to intersect the original object plane AC in D, and adopting a similar procedure to that given for the case of axial aberration,

the aberrations of the imagery of F may be given in terms of ω_D, the aberrations $\omega_{P(\bar{u})}$ and $\omega_{P(\bar{u}+\gamma)}$ of the axial pupil-point P for aperture angles APC $=\bar{u}$ and APD $=(\bar{u}+\gamma)$, and the quantity Δn(QR) where Q and R are the intersections with DP of circles through F centred on P and D,

$$\omega_F=\omega_D+\omega_{P(\bar{u}+\gamma)}-\omega_{P(\bar{u})}-\Delta n(\mathrm{QR}). \qquad \ldots\ldots(9)$$

Inserting the first-order values and equating coefficients, eqns. (6) result.

The variations of the first-order chromatic aberrations may be treated similarly, and since in this case the order of magnitude considered is that of the second power only of the aperture and field, the quantities Δn(QR) are negligibly small. Denoting the chromatic aberration of the imagery of C for some specified wavelength variation by $\omega_C=\frac{1}{2}\Sigma C_I+\Sigma C_{II}$ where $\frac{1}{2}\Sigma C_I$ is the longitudinal and ΣC_{II} the transverse chromatic aberration, and writing $\frac{1}{2}\Sigma\overline{C_I}$ for the longitudinal aberration of the pupil point for a field angle $\bar{u}$, then by eqn. (9), to the order of accuracy required,

$$\tfrac{1}{2}\Sigma C_I^*+\Sigma C_{II}^*=\tfrac{1}{2}\Sigma C_I+\Sigma C_{II}\frac{\bar{u}+\gamma}{\bar{u}}+\tfrac{1}{2}\Sigma\overline{C_I}\left[\left(\frac{\bar{u}+\gamma}{\bar{u}}\right)^2-1\right]+\tfrac{1}{2}H\Delta\left(\frac{\delta n}{n}\right)\frac{\gamma}{\bar{u}},$$

or, equating the parts involving equal powers of the field angle,

$$\left.\begin{aligned}\Sigma C_I^*&=\Sigma C_I+(\gamma/u)\Sigma\left[2C_{II}+H\Delta\left(\frac{\delta n}{n}\right)\right]+\left(\frac{\gamma}{\bar{u}}\right)^2\Sigma\overline{C_I}\\ \Sigma C_{II}^*&=\Sigma C_{II}+(\gamma/\bar{u})\Sigma C_I,\end{aligned}\right\} \qquad \ldots\ldots(10)$$

where, for a symmetrical system of spherical surfaces (see, for example, Hopkins 1950) $\Sigma C_I=\Sigma Ay\Delta(\delta n/n)$, $\Sigma C_{II}=\Sigma C_I\bar{A}/A$, δn being the change of index of each medium for the wavelength range considered, and as before, in eqn. (10) $\gamma/\bar{u}=\bar{H}\delta\bar{E}$.

The variation of the first-order aberrations with stop position may readily be treated by the same general method, and the first three of eqns. (4) may be shown in this way to be valid, not only for any symmetrical system of reflecting or refracting surfaces, but for any system having axial symmetry and isotropic object and image spaces.

§ 3. CONCLUSIONS

(i) *Invariance of Aberrations*

The conditions for the invariance of the Seidel aberrations for changes of conjugates follow immediately from eqns. (6) and, while each aberration separately may be made zero and invariant for all magnifications, it is clear that this cannot be achieved for all the coefficients simultaneously in a lens of finite power. Various combinations of invariance are possible.

Distortion is invariant if the spherical aberration of the pupil point is zero, and astigmatism if in addition $(S_V+H\Delta\bar{u}^2)=0$; a lens having invariant astigmatism has therefore invariant distortion, and this astigmatism can only be zero if the stop is in the nodal plane, so that $\Delta\bar{u}^2=0$; this problem was partially treated by Merté (1920). For a lens with its stop at the node, $H\Delta\bar{u}u$ may be written $-H^2/nf'$, where n is the refractive index of the object space and f' the image space focal length. For a system with object and image space of air the three conditions for invariant coma are then $\overline{S_I}=0$; $3S_V+H\Delta\bar{u}^2=0$;

$3S_{III}+PH^2-KH^2=0$. For a system having zero and invariant distortion and astigmatism the first two conditions are satisfied, and the third, which is the condition for the coma to have a stationary value, reduces to equality of power and Petzval curvature, and cannot be achieved for a lens of finite power having a flat field.

The four conditions for invariance of spherical aberration are $\overline{S_I}=0$; $4S_V+3H\Delta\bar{u}^2=0$; $6S_{III}+2PH^2+3H\Delta u\bar{u}=0$; $4S_{II}+H\Delta u^2=0$. Since the spherical aberration is independent of the stop position, the aberration of the pupil point is necessarily included in the range of invariance, and hence the coefficient S_I can only be invariant if it is zero. Since Δu^2 varies with the conjugates, being zero only at unit magnification, the last condition requires that the coma can only be zero at this magnification, corresponding to the incompatibility of the sine condition and Herschel's condition at other positions.

The combinations of invariance of the primary aberrations which are theoretically possible are also physically realizable. Thus process lenses are made having invariant and corrected distortion astigmatism and field curvature; such lenses have coma changing linearly with $\overline{H\delta E}$, and spherical aberration stationary at unit magnification. For thin lens systems at the stop, distortion and astigmatism are invariant, and the number of conditions for invariance of coma and spherical aberration reduces to one and two respectively. The condition for invariance of coma is satisfied, for example, by a thin Mangin mirror system of refractive index 1·620 whose air–glass surface is in the aplanatic condition at unit magnification, where the spherical aberration is corrected, and stationary. The conditions for invariance of spherical aberration may be satisfied by giving a thin system of mirror and meniscus lens of appropriate powers to make $6S_{III}+2PH^2-3KH^2$ zero a shape to correct the spherical aberration of the whole.

For the primary chromatic aberrations the invariance conditions given by eqns. (10) are very simple. Thus transverse chromatic aberration is invariant if the chromatic aberration of the pupil point is corrected; and if the object and image spaces are of the same material, longitudinal colour is stationary if the transverse chromatic aberration be corrected, and invariant if, in addition, this transverse aberration is invariant.

(ii) *Correction for more than one Magnification*

Since spherical aberration is normally corrected for four sets of conjugates, coma for three, and astigmatism for two, the conditions that these conjugate surfaces may coincide for different aberrations may be formulated. Since distortion is normally only corrected for one pair of conjugate planes and, if it is invariant, the number of corrected magnifications for each of the other aberrations is reduced by one, distortion correction is not compatible with the conditions to be considered.

Considering first the simultaneous correction for two magnifications of astigmatism, coma, and spherical aberration, since, when these are corrected, they and S_V are all invariant with stop position, the stop may, without loss of generality, be taken at the node, $\overline{S_I}$ then referring to the aberration at this stop position, and the conditions required, from eqns. (6), are then

$$2S_V^2=\overline{S_I}(PH^2-H^2/nf'),2S_VH^2/nf'=-\overline{S_I}H\Delta u^2. \quad \ldots\ldots(11)$$

It follows that the second conjugates for which the lens is corrected must have an angular magnification which is the reciprocal of the first, and that the distortion is equal and opposite in the two positions, and that the coefficient $\overline{S_I}$ must be of opposite sign to the power of the system if the field curvature is zero. For a lens corrected at a given angular magnification, the values of S_V and $\overline{S_I}$ required to give correction at the reciprocal magnification may thus be calculated and, for the practically interesting case of a lens in air corrected for field curvature and a real object and image, the resulting values are so large as to be unattainable in systems of normal construction, requiring surfaces which are either extremely deeply curved or at relatively large distances from the nodes; thus, S_V and $\overline{S_I}$ have their minimum values for real conjugates if the lens is corrected for an object at infinity and at the front principal focus, and in this case $S_V = \pm H^3/y^2$, $\overline{S_I} = 2H^4/y^4K$, corresponding, for a field angle $\bar{u} = \frac{1}{2}$, to a distortion of 87·5% and a spherical aberration of the pupil point of 600 wavelengths per inch of focal length.

In considering this problem of a system giving aberration-free imagery for two pairs of conjugates, Hertzberger and T. Smith, in papers already referred to, have stated that Maxwell's Proposition IX was in error; this proposition is that "It is impossible, by means of any combination of reflexions and refractions, to produce a *perfect* image of an object at two distances, unless the instrument be a telescope, and $l = n = \mu_1/\mu_2$, $m = l'$" (l, m, and n being the transverse, longitudinal and angular magnifications, and μ_1, μ_2 the refractive indices of the object and image spaces). This disagreement appears to be due to the fact that Maxwell's definition of a perfect image, given at the beginning of his paper, is one having perfect definition and freedom from field curvature and distortion, which is not the case for the systems considered by Herzberger and Smith. With Maxwell's definitions, his proposition is correct. This does not of course invalidate Smith's refutation of Maxwell's later statement that "we cannot get perfectly focused images of an object in two positions even at the expense of curvature and distortion".

A further case of possible interest is the simultaneous correction of coma and spherical aberration for three sets of conjugates. Here again, if S_I and S_{II} are zero they and S_{III} are unchanged by a change of stop position, and this may therefore be taken at the node without loss of generality, S_V and $\overline{S_I}$ then referring to the values of these coefficients for this stop position, and the two conditions to be fulfilled are

$$\overline{S_I}(3S_{III} + PH^2 - 2H^2/nf') = 3S_V^2,\ S_V(3S_{III} + PH^2 - H^2/nf') = \overline{S_I}H\Delta u^2. \quad \ldots(12)$$

If $S_{III} = 0$, these reduce to equations which are clearly incompatible with eqns. (11) for a system of finite power and flat field, so that such a system cannot simultaneously have a flat field anastigmatism correction for two pairs of conjugates and be aplanatic for a third pair. It may be shown that, for real object and image distances for all three conjugates, S_V and $\overline{S_I}$ have minimum values if for one set of conjugates the object be at infinity and the other two coincide at the front principal focus, or vice versa, and in this case S_V has the same value as for the anastigmat corrected for two pairs of conjugates, and $\overline{S_I}$ has three-quarters of the value for that case; as before, therefore, these are so large as to be virtually unattainable practically.

REFERENCES

BOEGEHOLD, H., and HERZBERGER, M., 1935, *Compositio Mathematica*, **1**, 448.
GRENAT, H., 1949, *Rev. Opt. (Théor. Instrum.)*, **28**, 389.
HERZBERGER, M., 1931, *Strahlen Optik* (Berlin : Springer) ; 1946, *Ann. N.Y. Acad. Sci.*, **48**, 2.
HOPKINS, H. H., 1950, *Wave Theory of Aberrations* (Oxford : University Press).
LONGHURST, R. S., 1950, *Thesis*, University of London.
MAXWELL, J. CLERK, 1858, *Quart. J. Pure Appl. Math.*, II, and *Sci. Pap.*, **1**, 271.
MERTÉ, W., 1920, *Z. Phys.*, **1**, 174.
SCHWARZSCHILD, K., 1905, *Abh. kgl. Ges. Wiss. Göttingen, Math.-phys. Kl.*, **4**, No. 1.
SLUSSAREFF, G., 1941, *J. Phys. U.S.S.R.*, **4**, 537.
SMITH, T., 1948, *Proc. Phys. Soc.*, **60**, 293.
WYNNE, C. G., 1949, *Proc. Phys. Soc.* B, **62**, 772.

Propagation of Ultrasonic Waves in Vapours near the Critical Point

BY H. D. PARBROOK* AND E. G. RICHARDSON
King's College, Newcastle upon Tyne

MS. received 19*th October* 1951, *and in amended form* 14*th January* 1952

ABSTRACT. An experimental study is made of the velocity and absorption of ultrasonic waves in carbon dioxide and ethylene at frequencies between ½ and 2 Mc/s and at pressures up to 100 atmospheres in a variable-path acoustic interferometer. At pressures above 10 atmospheres the results are independent of frequency (in this range) in the gaseous phase. The velocity and absorption coefficient reach a minimum near the condensation point, but especially at the critical point itself have high and indeterminate values when the change of phase takes place. The ultrasonic viscosities calculated from these measurements are of the order of 1 000 times those derived from transpiration or low-frequency oscillation experiments.

§1. INTRODUCTION

EXPERIMENTAL work on the propagation of ultrasonic waves in various gases has given results for ultrasonic velocities and absorption coefficients which cannot be adequately explained by the 'classical' theories of sound propagation. Generally, for given pressure and temperature conditions, there is, at certain frequencies, a dispersion of velocity accompanied by a sharp increase in absorption at that frequency. Experiment shows that an increase in pressure or temperature displaces the dispersive region to higher frequencies. However, with few exceptions, previous workers on the effect of pressure on ultrasonic velocity and absorption in vapours have covered only a limited range of pressure about the normal.

It was the intention in this research to make measurements in one or two vapours at such temperatures and pressures that the transition to the liquid state would be covered and, in particular, to investigate the variation in the absorption coefficient α in this region. It is well known that the coefficients of variation of viscosity with temperature run conversely in the two states, so that information of this kind should show whether the viscosity which characterizes ultrasonic

* Now at the University of Liverpool.

absorption follows a similar trend. For convenience, carbon dioxide and ethylene were chosen as they have critical temperatures not far removed from the temperature of a laboratory. The research was conducted as a study of ultrasonic propagation in the neighbourhood of the critical state and not, intentionally, as a study of the molecular properties of individual vapours.

Most of the experiments were made on carbon dioxide, with a small number on ethylene. The well-known dispersion of velocity V in carbon dioxide at atmospheric pressure was absent at higher pressures over the range of frequencies used here. At all three frequencies, single isothermals for velocity plotted against the quotient frequency/pressure were obtained. Ethylene also shows some dispersion at pressures near atmospheric, but to a much less extent. In fact, both the vapours used in these experiments showed similar ultrasonic properties, having regard to the location of their respective critical points, so that extensive work on ethylene proved unnecessary for our purpose.

Previous work on these vapours under high pressure is confined to velocity and a few frequencies only. Spakowski (1935) made measurements in carbon dioxide near the critical point at a frequency not stated, although from the description and size of the apparatus one judges it to have been in the audible range. Herget (1940) has measured velocities at one ultrasonic frequency of about 280 kc/s in carbon dioxide (5 to 98 atm) and ethylene (35 to 75 atm) at temperatures near their respective critical points. Finally, Noury (1946) quotes some velocities in what he describes as impure 'war-time' carbon dioxide.

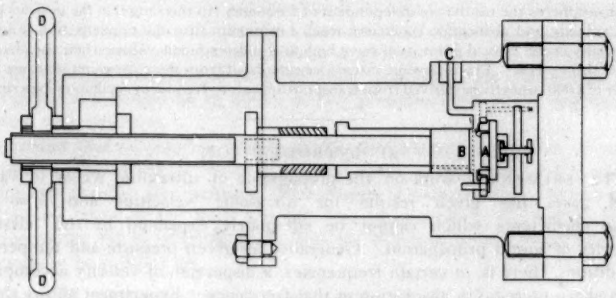

Fig. 1. Section of interferometer.

§2. APPARATUS

A single quartz acoustic interferometer was used for the measurement of velocity and absorption in gases and liquids under high pressures.

Figure 1 shows the final design of pressure vessel used. The main vessel contains the quartz transducer A, facing the reflector on its piston B, in a chamber to which the gas is introduced by a port C. The piston is moved by the large screw-head D whose setting is measured optically. There is a second gas chamber and piston of suitable size to compensate for changes in volume as the main piston moves. The whole apparatus is surrounded by a lagged enclosure.

A platform into which the crystal holder is locked is mounted in the vessel by three spring-loaded bolts. This permits parallel adjustment of the transducer face and reflector.

The sources were X-cut crystals with plated electrodes, mounted so that the quartz merely rests in a tufnol cup on a brass bed-plate machined as flat as possible, heavily chromium-plated and then polished to a near optical flat. A pigtail of 0·001 in. diameter platinum wire makes contact with the upper surface.

The crystals were discs cut wide relative to their thickness to limit errors due to diffraction. The ratio of radius R to thickness (or wavelength) did, in fact, increase at the highest frequencies. Losses due to diffraction, if they had occurred, would have been apparent as an increase of α at the lower frequencies, but such was not the case.

Though an examination of the wave-forms during a 'run' will show whether or not source and reflector are accurately parallel, an initial test was made in which this system formed part of a Michelson interferometer so that the parallel movement would be assured to within a light wavelength. This is unnecessarily precise for the present purpose, but the necessity for parallelism cannot be over-emphasized if accurate values of absorption are to be attained, since otherwise satellite peaks or cols in the reaction wave-form are obtained. The initial adjustment to ensure that the reflector face is parallel to the quartz (before the base-plate is clamped on) is made with a depth gauge and the final test by observing the acoustic wave-form. It may not be possible entirely to eliminate satellites by such parallel adjustment if transverse resonances of the fluid in the tube are excited, as Bell (1950) has shown, but the fact that the accepted values of absorption in air were obtained in this apparatus indicated the absence both of this effect and of variations in phase and attenuation coefficient due to the consequent three-dimensional standing waves.

The crystals were driven by a Hartley oscillator of conventional pattern, which gave stability within ± 1 c/s over the time of one run (about 7 minutes) up to a frequency of 4 Mc/s. A frequency meter, checked from time to time against B.B.C. transmissions, accurate to 1 in 10^7, was loosely coupled to the oscillator. The frequency changed slightly under pressure. Consequently the frequency ascribed to each isothermal curve of V and α in the sequel is to be considered as the mean for the curve in question.

§3. FILLING THE VESSEL

Gas in cylinders supplied with special attention to the absence of air as an adulterant is stated to be better than 99·7% pure. As explained in the Introduction, our concern was to have the gas free from any adulterant which might cause dispersion of velocity specific to its presence and consequent 'relaxational absorption'.

The possible impurity most likely to do this is water vapour. However, attempts to remove the last traces of water vapour by drying agents or to add further water vapour (in one special test) produced no change at s.t.p. in the dispersion or absorption over the working range of frequency. At higher pressures, as will appear, these phase and attenuation factors become independent of frequency, at least as far as the gaseous state is concerned, in the range of frequency employed. Nevertheless, these s.t.p. tests—by comparison with the known results of other workers in carbon dioxide—serve as useful checks on the purity of the gas supplies.

The bomb was evacuated and connected to the cylinder. To obtain pressures up to 120 atm the gas cylinder was carefully heated before it was cut off from the bomb. The Bourdon gauge, duly calibrated, gave the pressure of the gas inside the bomb.

Temperatures over the range 0°–40° C were attained in the lagged enclosure by circulating air which had been fanned over electric heaters (for carbon dioxide) or drikold (for ethylene) as the case may be. The thermostat for the enclosure is a toluene regulator fitted with a Sunvic proportioning head. The regulator controlled the heater through an electronic relay. With this arrangement it was possible to hold the gas temperature, shown by thermocouples, inside the bomb to 0·02° C. A high grade of stability in pressure and temperature is, of course, necessary near the critical point.

§4. METHOD OF MEASUREMENT

The conditions under which the attenuation in the gas column can be derived from the logarithmic decrement of the peaks of anode current I in the driving circuit as the reflector is moved have been laid down by Hardy (1943). The somewhat different conditions for a liquid—due to the more nearly matched impedance of fluid and solid reflectors—have been discussed by Fox (1937). Hardy shows that errors in the absorption coefficient α will not exceed 2% if the ratio $\delta I/I$ is less than 0·03, where δI is the change in anode current as the

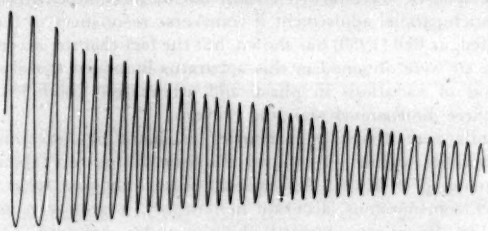

Fig. 2. Peaks in anode current with change of path length.

reflector is moved from a position of maximum to a position of minimum. To measure small changes in I a shunted galvanometer with ' back-bias ' arrangement was used. Battery supplies were used throughout.

Automatic recording of the galvanometer on a moving-paper camera was used to eliminate personal errors in reading the moving galvanometer light spot and to permit a constant check of wave-form.

The cylindrical lens in front of the camera has a series of lines engraved on its face. With a suitably disposed small filament lamp the photographic paper can be fogged except where these engraved lines cast a shadow. By arranging that this light fogs the paper before the exposure due to the galvanometer light—a question of orientation of lamps only—the initial photographic threshold of the paper is exceeded and an adequate exposure with the available reflected light obtained. Variable resistances and switches in series with these two lights give control of exposure times.

Figure 2 gives a typical run as recorded by this means. The speed of displacement of the reflector was considerably reduced at the beginning, middle and end of the trace. (The slightly smaller peaks obtained at other points in the trace are due to the motor 'overrunning' the response of the galvanometer.)

The absorption coefficient between two peaks corresponding to two reflector distances l_1 and l_2 was calculated from

$$\frac{\delta I_1}{\delta I_2} = \frac{\sinh 2\alpha(l_1+\beta)}{\sinh 2\alpha(l_2+\beta)} \simeq \exp 2\alpha(l_2-l_1)$$

for sufficiently large values of αl (β depends on the reflection coefficient).

In the actual mode of operation of the apparatus the gas was introduced at the highest pressure, left to attain the desired temperature, the various circuits put into operation and a run made at this pressure. Then the pressure was reduced by allowing some gas to leak slowly into an evacuated vessel and another run made, when pressure and temperature stability was regained.

§ 5. RESULTS

The velocity results in carbon dioxide are plotted in two stages. In fig. 3 are shown the (V, p) relationships: straight lines well below the critical

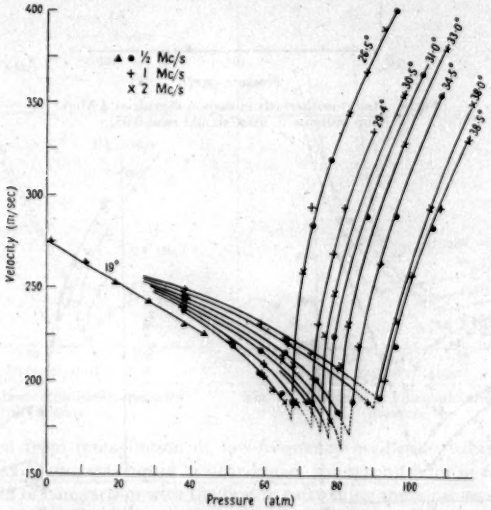

Fig. 3. (V,p) isothermals in carbon dioxide.

point and curving down to cusps at the critical point itself. They are in general agreement with Herget's results at 280 kc/s. The frequencies used were ½, 1 and 2 Mc/s; the velocities were found independent of frequency in the gaseous phase at all pressures above 10 atmospheres.

The absorption results in carbon dioxide are shown in fig. 4 and in ethylene in fig. 5 in terms of the absorption per wavelength μ. As already stated, fewer measurements were made with ethylene, but fig. 5 shows typical results for both V and μ in this substance at $\frac{1}{2}$ Mc/s. The velocity in this gas is also found independent of frequency, when Herget's few results are added to ours.

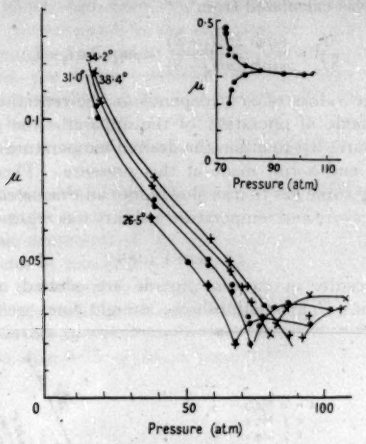

Fig. 4. (μ, p) isothermals in carbon dioxide at $\frac{1}{2}$ Mc/s. (Top ordinate in inset should read 0·05).

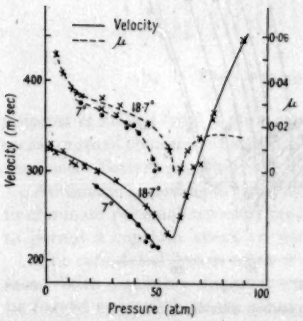

Fig. 5. Isothermals in ethylene at $\frac{1}{2}$ Mc/s.

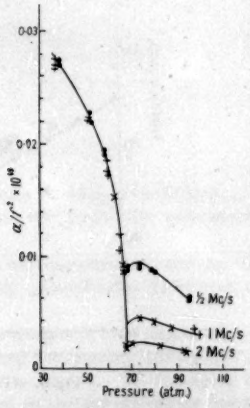

Fig. 6. $(\alpha/f^2, p)$ curves in carbon dioxide at 26·5° c.

Figure 6 shows the constancy of α/f^2 in the gaseous régime, but discrete curves for the different frequencies in the liquid state, in which, however, the accuracy of measurement is less than in the gaseous state.

When by chance the conditions corresponded exactly to the point of transition, the reaction on the source failed completely, due to the very high absorption; this may be ascribed to scattering by the striated masses of indeterminate fluid known to exist in this regime. Proceeding, as usual, from the liquid towards the gaseous phase, sometimes a rise, sometimes a fall was encountered in μ just before the transition (cf. inset to fig. 4). In the former case, the absorption after reaching a value impossible to measure dropped sharply to a point on the curve proper to the gaseous phase. Schneider (1951) has drawn attention to the very large attenuation at the critical point itself.

§6. COMPARISON OF ULTRASONIC AND STEADY-FLOW VISCOSITIES

According to the Helmholtz–Kirchhoff formula, the absorption coefficient α in a gas at pulsatance ω should be related to the kinematic viscosity ν, thermal diffusivity κ and ratio of specific heats χ by

$$\alpha = \frac{\omega^2}{2V^3}\{\tfrac{4}{3}\nu + (\chi - 1)\kappa\}.$$

When, however, we attempt to deduce from our data the variation of ν with p using this formula we find very large values (fig. 7) in comparison with values

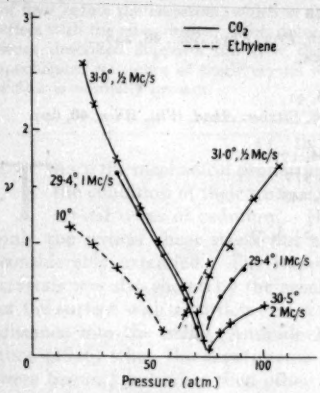

Fig. 7. Variation of ultrasonic viscosity with pressure.

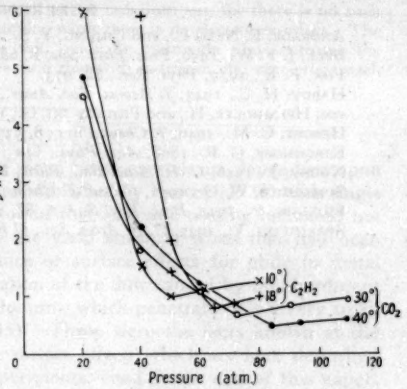

Fig. 8. Variation of kinematic viscosity with pressure.

of ν deduced from transpiration or low-frequency oscillation values. As the state of the substance was liquid or near-liquid, the second term in the brackets was neglected in comparison with the first in calculating these values of ν.

Phillips (1912) gives values of viscosity in carbon dioxide under pressures and temperatures close to the critical point. These were obtained from flow experiments in capillary tubes. As there seemed to be no corresponding published values for ethylene (except at constant density) it was decided to obtain them from the damping of a vessel filled with the fluid oscillating about an axis of suspension in a vacuum. This method, suggested by Helmholtz and Piotrowski (1860), was refined into an absolute method by Andrade and Chiong

(1936). A comparative method was used, with the gas cylinder itself (10 in. × 3in.) held by a bifilar suspension so that it could be gently set in oscillation—through the intervention of electromagnets—about its axis, set vertically. The whole was mounted in an evacuated glass cylinder and this again in a thermostat, the damping of the oscillations being recorded optically. Afterwards, the cylinder was filled with a fluid of known viscosity and the damping again measured for the purpose of calibration.

The results of such experiments on ethylene and carbon dioxide at the critical temperature are shown in fig. 8, using Amagat's density values. It is at once apparent on comparing these curves with those of fig. 7 that the viscosities deduced from the ultrasonic attenuation using Kirchhoff's formula (1868) in this region are about 1 000 times greater, though the general trend of the curves is reproduced.

It is interesting to note that although the actual values of the coefficient for gases under pressure are much higher than those deduced from Kirchhoff's theory they follow the same variation with pressure, as is indicated by his equation.

It may be remarked that 'condensed gases' at low temperatures such as liquid argon and helium show absorption coefficients of the same order as do these vapours in the critical region.

REFERENCES

Andrade, E. N. da C., and Chiong, Y. S., 1936, *Proc. Phys. Soc.*, **48**, 247.
Bell, J. F. W., 1950, *Proc. Phys. Soc.* B, **63**, 958.
Fox, F. E., 1937, *Phys. Rev.*, **52**, 973.
Hardy, H. C., 1943, *J. Acoust. Soc. Amer.*, **15**, 91.
von Helmholtz, H., and Piotrowski, G., 1860, *Sitzber. Akad. Wiss. Wien*, **40**, 607.
Herget, C. M., 1940, *J. Chem. Phys.*, **8**, 537.
Kirchhoff, G. R., 1868, *Ann. Phys., Lpz.*, **134**, 177.
Noury, J., 1946, *C. R. Acad. Sci., Paris*, **223**, 377.
Schneider, W. G., 1951, *Canad. J. Chem.*, **29**, 243.
Phillips, P., 1912, *Proc. Roy. Soc.* A, **87**, 48.
Spakowski, V., 1935, *C. R. Acad. Sci., U.R.S.S.*, **3**, 31.

The Influence of Electrolytes on the Mechanical Properties of Certain Metal Single Crystals

By E. N. da C. Andrade* and R. F. Y. Randall†
Department of Physics, University College, London

MS. received 6th March 1952

ABSTRACT. The contact of electrolytes has a marked effect on the mechanical behaviour of single crystals of cadmium and zinc which have been exposed to the air. This is due to the disruption, or formation, of a thin surface film, probably of oxide or hydroxide. If ordinary single crystal cadmium wires are loaded so as to flow very slowly, the contact of solutions containing free cadmium ions increases the rate of flow: a similar effect exists in the case of zinc treated with solutions of zinc salts. If the surface of the wire is cleaned by preliminary thermal evaporation there is no such effect, establishing that it is due to a surface film normally present. Solutions of cadmium or zinc nitrate stop the flow and raise the critical shear stress appreciably, which is attributed to the formation of a surface film, probably of hydroxide. With the cadmium nitrate there is a temporary increase of flow before the cessation, which is attributed to the cadmium ion, for there is no such effect with the zinc nitrate. With polycrystalline wires there is no electrolyte effect. The work described supports the view that a thin oxide or hydroxide film increases the mechanical resistance of single crystal wires, and that with cadmium and zinc wires such a film is normally present.

§1. Introduction

That the mechanical properties of metal single crystals are dependent upon the condition of their surface was established by Roscoe (1936) with single crystal wires of cadmium. He found that an oxide coating increased not only the critical shear stress but also the yield stress of wires that had been considerably extended. The importance of surface effects for glide in metal crystals was also shown by the acceleration of the flow caused by bombardment of the surface with α particles from polonium, which penetrate only a very small distance into the metal (Andrade 1945). These were the facts known at the time (1946) when the experiments on surface effects which are here described were begun,‡ but since then other experiments, cited at the end of this paper, have emphasized the influence of surface conditions.

The original intention was to find the effect on the mechanical properties of a single crystal wire of (*a*) removing a thin layer of the surface, (*b*) adding a thin layer of metal to the surface, both by electrolysis. Experiments on these lines, however, showed that the electrolyte alone, without applied potential difference, had marked mechanical effects. Accordingly the effect of the contact of various electrolytes on the flow of single crystal wires of cadmium was investigated: a few experiments have since been carried out with zinc. The general result has been to bring evidence as to the important effect of surface

* Now Director of the Davy Faraday Laboratory, The Royal Institution, London.
† Now at The University of Sheffield.
‡ Publication has been delayed by a variety of causes, particularly by both the authors leaving the University College Physics Laboratory, where the experiments on cadmium were carried out, in 1949.

films on the mechanical properties of single crystals, which has also been emphasized by the recent work of Harper and Cottrell (1950). Some electrolytes disrupt a coating of oxide or other surface contamination already existing, and so make the crystal more prone to flow: others lead to the formation of a coating on a previously cleaned surface, or thicken the coating on an ordinary surface, in both cases notably raising the critical shear stress.

§2. PREPARATION AND TESTING OF SINGLE CRYSTAL WIRES

The crystals were made from 1 mm diameter spectroscopically pure wire, drawn by Messrs. Johnson and Matthey from cast rods which had been selected as free from cavities. Such cavities, containing air or other gas, remain during drawing and lead to uneven surface oxidation in the single crystals. The impurity of both cadmium and zinc was less than 0·001% and consisted chiefly of lead. A few crystals were made from cadmium of commercial purity; these

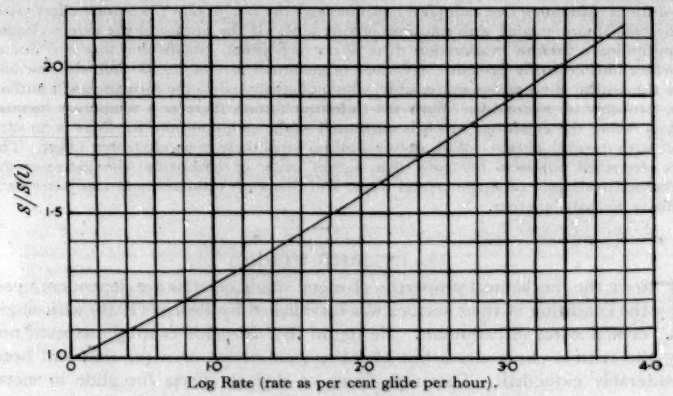

Fig. 1. Critical shear stress, for spectroscopically pure cadmium single crystal, as a function of log rate.
$S(1)$ = Stress for 1% per hour.

gave a critical shear stress of 30 g wt/mm², as against 16 g wt/mm² for the spectroscopically pure metal, both at an initial rate of flow of 0·02% glide per minute. This value of the critical shear stress compares well, as determinations of critical shear stress go, with the value of 13 g wt/mm² given by Andrade and Roscoe (1937) at the same rate of glide. Since critical shear stresses from cadmium are quoted at widely different rates of flow, which leads to confusion, we give in fig. 1 a curve for spectroscopically pure metal connecting critical shear stress, expressed in terms of that giving a glide of 1% per hour as unity, with log rate of glide in per cent per hour, calculated from the formula given by Andrade and Roscoe (1937, p. 164), which has been found to give a very satisfactory representation of the experimental facts. At a glide rate of 1% per second, for instance, the critical shear stress is 27 g wt/mm² if that for 1% per hour is taken as 13 g wt/mm². The critical stress for the spectroscopically pure zinc was found to be 33 g wt/mm² at the rate of glide of 0·02% per minute.

The wires were transformed to single crystals by the travelling furnace method of Andrade and Roscoe (1937). The polycrystalline wire was cleaned with metal polish and a degreasing agent and then, by means of a special apparatus, transferred without admission of air to an evacuated Pyrex tube which had been cleaned and baked out under vacuum conditions for half an hour at 400° c. In such Pyrex tubes, in which they were held loosely, the wires were sealed off at a pressure of 10^{-4} mm Hg. Several of these tubes were contained in a horizontal silica tube of about 1 cm internal diameter passing through the furnace, which, drawn by a wire controlled by a synchronous motor, travelled along it without touching at a rate of about 4 cm per hour. The temperature of the furnace was maintained constant to within 1·5° c. At either end of the furnace was fixed a small compartment, kept cold by running ice water, which ensured that the temperature gradient was constant. The whole was carefully shielded from draughts. Crystals of any desired orientation were produced by fusing a short length of crystal of this orientation to the wire to be transformed.

Special precautions against strain were taken in the transfer of the very soft single crystal from the tube to the extensometer system, which was accomplished by means of a specially designed geometric slide.

The crystal orientation was determined to within 1° by back-reflection x-ray photographs and the use of a Greninger chart. In the earlier work the crystals were tested at 1 cm intervals along the wire; it was found, however, that crystals made in the way described, which gave sharply defined spots in Laue photographs, were homogeneous and accordingly in later work only one photograph was taken for orientation.

§3. EXPERIMENTS ON PLATING WITH CADMIUM

The commercial plating solution used* contained cadmium potassium cyanide, potassium cyanide, sodium carbonate and caustic soda. In the experiments on the effect of plating the surface a control wire was cut from the same single crystal wire as the specimen to be plated. This latter was fixed vertically in the plating bath on the axis of a cylindrical rotating anode, which was provided with vanes for stirring. When the plating process had continued for three hours at a current strength that gave a calculated depth of coat of about 10^{-5} cm, the wire was removed, washed in distilled water, dried in air, and then mounted in the holder with the precautions already described. The crystal orientation was measured and the specimen transferred to the extensometer.

With the control specimen the load was increased by 2 g wt every 5 minutes until a slow rate of flow (about 0·01% to 0·1% per minute) was produced and measured. The plated specimen was then tested under the same loading routine and the rate of flow compared with that of the plated specimen. In the case of eight crystals out of twelve a markedly greater rate for the plated specimen was observed, the three highest values of the ratio to that of the control being 10, 12 and 17. However, the results were irregular and in three cases there was actually a decrease of rate, which in the light of subsequent experience we attribute to oxidation having taken place in the drying process. Since a few control experiments showed that leaving the wires in the electrolyte, without passing any current, produced an increase in rate, subsequent experiments were carried out under the simpler conditions.

* Supplied by Messrs. Canning & Co., Ltd.

§4. INFLUENCE OF CONTACT OF ELECTROLYTES

To avoid subsidiary electrolytic effects the extensometer, shown in fig. 2, was made of plastic (distrene). The disc AA rested on the edge of a thick glass beaker which had been ground smooth, and was held down by weights, not shown. To it was attached by three vertical columns, of which one is shown at B, the base C, on which was mounted the chuck D, in which the lower end of the specimen, about 6 cm long, was gripped in two V-shaped cuts by plastic screws. The upper end of the specimen was held in a chuck F, attached by two threads GG to the pulley wheel P which ran in a ball race, the axis being held in the V's of the support H. The light scale pan S, attached by a single wire

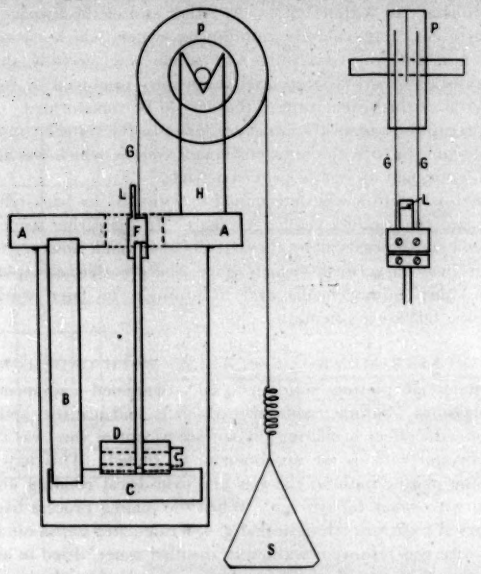

Fig. 2. Apparatus for straining single crystals in contact with electrolytes.

to the pulley wheel, counterbalanced the chuck F and carried the weights by which the tension was applied. The friction was very small, amounting at most to 1% of the total load. The attachment L to the upper chuck carried a fiducial mark, allowing the extension of the specimen to be read by a cathetometer graduated in $\frac{1}{100}$ mm.

The method of testing was to increase the load in small steps until a slow rate of flow was produced and then, after this rate had been measured for a period of, say, 20 minutes, to introduce the electrolyte and measure the subsequent flow. The ratio R of the rate after contact of electrolyte to the rate before contact of electrolyte was taken as a measure of the effect. This is a very sensitive method, as the rate of flow is greatly influenced by small changes in structure or local stress.

The first experiments were done with the commercial plating solution with which the preliminary plating experiments had been carried out. Wires of various crystal orientation were used. Immediate increases of rate, with values

of R up to 15 were found, but once more the values of R were very variable and did not appear to be related to the crystal orientation. It was decided to work with simple electrolytes.

The first electrolyte used was a nearly saturated solution of cadmium sulphate. Figure 3 represents a typical experiment, the angle ψ_0 made by the crystal axis with the glide plane being 28°.* Thirty-eight experiments were done in all, with various values of ψ_0 and with various amounts of pre-glide, from 0 to 80%. The values of R varied from 1·0 in three cases (which we now attribute to the probability that the surfaces were unexpectedly clean) up to 9·6: in 16 cases R was between 2 and 3·5. While the effect is marked, and always takes place immediately the electrolyte is brought into contact with the wire, it is variable

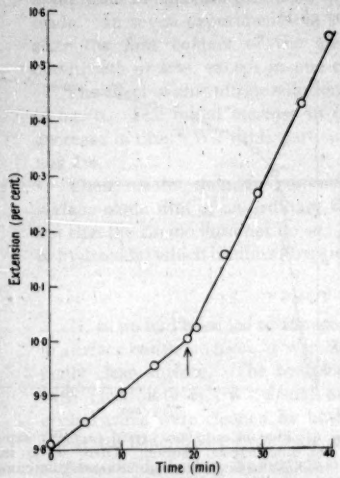

Fig. 3. Flow of cadmium crystal exposed to cadmium sulphate solution, introduced at moment indicated by arrow. Rate of extension before introduction of electrolyte, 0·01% per minute: after 0·026% per minute. In this and all related diagrams the arrow indicates the moment of introduction of the electrolyte.

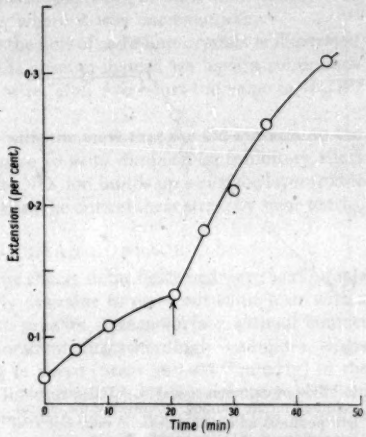

Fig. 4. Flow of zinc crystal ($\psi_0 = 28°$) exposed to zinc sulphate solution. The crystal was hardening at the time, indicated by arrow, when the solution was introduced.

in magnitude. However, something can be gathered by taking average values. Table 1 shows the average values of R for different ranges of initial angle ψ_0, the number of tests from which the average is taken being given. It will be seen that there is certainly no significant variation of R with ψ_0, since the slightly higher value of R for large values of ψ_0 is an average of two tests only.

Table 1

ψ_0	0 to 24°	25 to 44°	45 to 64°	65 to 80°
Average R	3·0	2·9	3·0	4·0
Number of tests	9	20	7	2

The grand average for R is 2·9.

* It may be remarked that for ψ_0 greater than 50° local flow may occur, owing to the relation between physical hardening and geometrical softening (see Andrade and Roscoe 1937, p. 159).

As regards the variation with pre-glide p, table 2 shows average values of R for different ranges of p, from which it seems clear that the effect is smaller for small pre-glides, but constant for pre-glides greater than 10%.

Table 2

Pre-glide (%)	0 to 9	10 to 24	25 to 49	50 to 80
Average R	1·4	3·3	3·4	3·4
Number of tests	8	10	16	4

It is not surprising that the hardening effect of the surface layer persists after glide has taken place, since Roscoe found that it was not very different after 300% glide from what it was at very small glide. The significance of the smaller value of R for very small pre-glide may be that the layer is more easily attacked by the electrolyte if it has already been disturbed by glide.

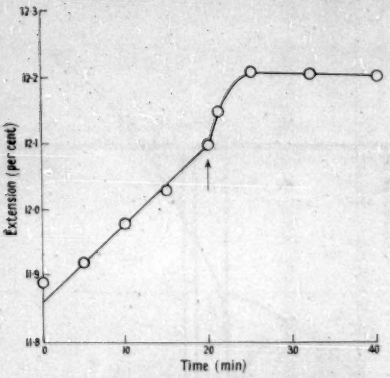

Fig. 5. Flow of cadmium crystal ($\psi_0 = 32°$) exposed to cadmium nitrate solution. Contact of the electrolyte produces an initial increase in rate, but after five minutes flow has practically ceased.

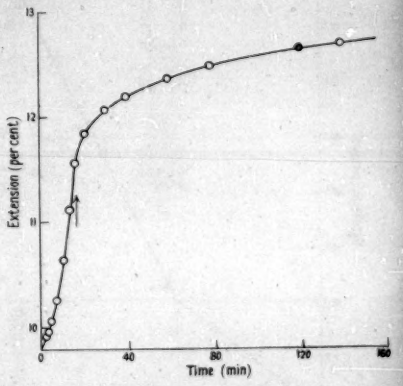

Fig. 6. Flow of cadmium crystal ($\psi_0 = 48°$) exposed to zinc nitrate solution. There is no initial increase in rate: the rate decreases continuously from the moment of contact.

With zinc crystals a similar increase of rate of flow was produced by the action of a concentrated solution of zinc sulphate. Figure 4 is an example, for zinc, in which the crystal was hardening at the moment when the solution was introduced, so that the value of R is very large.

A few experiments were carried out with cadmium single crystals and cadmium chloride, of the same molecular concentration as the sulphate, as electrolyte. They gave similar results. For what it is worth, with results showing a wide spread, the average value of R for the sulphate was 2·9 and for the chloride 2·5: the difference is not significant.

Experiments with cadmium sulphate solution carried out at 50° C showed no significant difference from those at 15° C, the average value of R for five trials being 2·1.

Nitric acid 1 in 500 gave $R = 1·6$ and nitric acid 1 in 50 gave $R = 7·0$.

Saturated solutions of cadmium cyanide and iodide had no effect on the flow of cadmium crystals, and water, used as a control, likewise had no effect.

So far the results recorded with electrolytes have been either negative (cyanide and iodide) or have been an immediate increase in rate of flow. With cadmium and zinc nitrate solutions, acting on cadmium single crystals, a new effect was found. Figure 5 shows a typical result with cadmium nitrate solution. There is an immediate increase in rate of flow, as with cadmium sulphate, but this is followed within five minutes by an almost complete cessation of flow. If the wire is left in the electrolyte for some time and subsequently tested, it is found that the load W_2 needed to produce the rate of flow that was produced originally, before the contact of the electrolyte, by a load W_1, has considerably increased. Thus in one experiment, after 40 minutes immersion, W_2/W_1 was 1·3, and after 16 hours immersion, in each of two experiments, it was 1·7, which is the kind of increase produced in Roscoe's experiments by an orange coat of oxide. In seven experiments on cadmium with cadmium nitrate, 30 minutes after the first contact of the electrolyte the rate of flow was reduced to one-fiftieth or less, except in one case, where it was one-twentieth.

The effect of zinc nitrate solution on the flow of cadmium crystals is illustrated in fig. 6. The initial increase in rate is absent: instead we have a continuous decrease in rate. With this particular wire, after two hours the value of W_2/W_1 was 1·4.

These results, then, are consistent with the view that the Cd ion acts on the surface oxide film of an ordinary Cd wire so as to diminish its inhibitory effect but that the Zn ion does not do so. The NO_3 ion builds up a surface layer (oxide or hydroxide) which inhibits flow and raises the critical shear stress by some tenths.

§5. EFFECT OF CLEAN SURFACE

If, as we had been led to suppose, the effects so far described were attributable to surface contamination, it was clearly desirable to carry out some tests with a really clean surface. The best way to prepare a clean surface without contact with electrolyte is by thermal evaporation and accordingly cadmium single crystal wires were cleaned by heating *in vacuo* (pressure $<10^{-4}$ mm Hg) in the apparatus described by Andrade and Randall (1950). A layer about 4×10^{-3} cm was removed, leaving the surface covered with pits, as described in the paper just quoted.

In a typical experiment a length of 6·5 cm was removed from a single crystal some 30 cm long and the remainder was surface-cleaned by evaporation. With the length removed a normal extension experiment was carried out with the apparatus of fig. 2, cadmium sulphate being used as the electrolyte. A section of the cleaned crystal was then placed in the extension apparatus and the load adjusted to give the same initial rate as with the uncleaned specimen, the interval between removal from the vacuum and the test being kept as small as possible. After 20 minutes flow at the chosen small rate the liquid was introduced.

Figure 7 shows a typical result. The rate ratio R is 1·5 for the normal surface: with the cleaned surface the introduction of the electrolyte does not affect the rate. In the following table are summarized the results of the eight experiments carried out. It will be seen that in no case was there any change of rate with the clean surfaces, while with the uncleaned crystals there was in all cases an increase in rate. That the rate ratio never exceeded 1·5 may be taken as an indication that the surface contamination was never bad.

In the case of the first two specimens there was a pre-glide of 30%, with the other specimens no pre-glide.

ψ_0, λ_0 are the angles initially made by the wire axis with glide plane and glide direction; R is the ratio defined on p. 448 for the ordinary crystals and R_c for the crystals surface-cleaned *in vacuo*; σ and σ_c are the respective critical shear stresses pertaining to the same initial rate of glide.

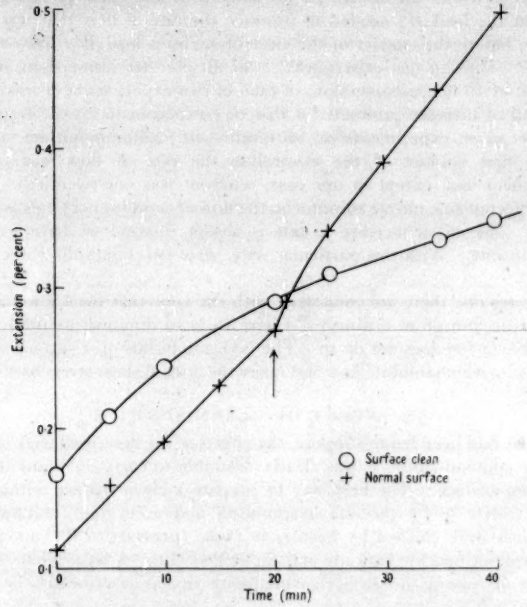

Fig. 7. Behaviour of surface-clean and normal cadmium crystal ($\psi_0 = 22°$) contrasted.

Table 3

ψ_0	λ_0	R	R_c	σ_c/σ
20	20	1·4	1·0	1·8
26	26	1·1	1·0	1·2
10	10	1·2	1·0	1·5
10	12	1·5	1·0	1·2
22	35	1·5	1·0	1·3
33	33	1·4	1·0	1·3
40	46	1·4	1·0	1·5
42	42	1·4	1·0	1·2

It will be observed that the critical shear stress is always higher for the clean-surface wire than for the normal wire. Andrade and Randall (1950) have attributed the pits formed by thermal etching to local spots of high free energy, where the vapour pressure is abnormally high. An alternative statement would be that thermal etching results in the removal of atoms which, owing to local

irregularity, are comparatively loosely bound. Since such local irregularity is likely to act as a source of dislocations, the rise of critical shear stress is understandable: local sources of weakness are boiled away.

§6. POLYCRYSTALLINE WIRES

A few experiments were made to see if there was any effect with polycrystalline wires. Tests on commercial cadmium wire of 1 mm diameter, with about 40 crystal grains to the diameter, failed to reveal any influence of the plating solution which had so marked an effect with the single crystal wire. The flow of polycrystalline zinc wire was likewise uninfluenced by zinc sulphate. Spectroscopically pure cadmium wire was annealed at 300°c until the grains had so grown that there were only one or two to the diameter. With this wire, owing to the large grain size, the extension was somewhat irregular; however, neither plating solution nor cadmium sulphate solution produced any observable increase in rate.

§7. DISCUSSION

The general result of these experiments, of which a preliminary note was published some time ago (1948), is to emphasize the great influence of surface layers of oxide, and/or possibly other salts, on the mechanical properties of single crystals, an effect which is particularly striking with silver crystals, as reported by Andrade and Henderson (1951). The absence of effect with a really clean surface, which has been confirmed by Menter and Hall (1950), seems to render it highly probable that the increased flow produced by suitable electrolytes is due to disruption of a film which tends to inhibit the propagation of sensitive dislocations from the surface, while the hardening action of both zinc nitrate and cadmium nitrate, which takes some time to establish itself in both cases, is due to the formation of a thin surface layer, which, according to Menter and Hall (1950), consists of cadmium hydroxide.

The immediate increase of flow caused by a solution of cadmium nitrate, which is not followed until later by the hardening, points to the cadmium ion as the effective agent in disrupting the surface film to which resistance is due. The contrast with the action of zinc nitrate, which produces from the start a progressively increasing hardening, points to the NO_3 ion as the effective agent in producing the hydroxide film.

It appears, then, that the action of solutions of cadmium sulphate and chloride is due to the cadmium ion. We are not fully clear as to the mechanism of the action, but probably the cadmium ion combines with the oxide or hydroxide component of the surface layer and so removes it into solution.

The lack of action of concentrated solution of cadmium iodide and cyanide can be explained, on the basis of views here put forward by the well-known fact that concentrated solutions of these salts give rise to very few Cd^{2+} ions. As shown by Riley and Gallafent (1932) the bulk of the metal in such concentrated solutions is present either as the undissociated molecule or as CdI^+ ions. A further point is that the greater ionization of the sulphate and chloride leads to greater hydrolysis

$$CdSO_4 + 2H_2O \rightleftharpoons Cd(OH)_2 + H_2SO_4$$

so that they would have a greater solvent action on a film of cadmium oxide than the iodide and cyanide.

Work by Raether (1950) on zinc crystals with freshly cleaved surfaces shows that any such surface exposed to air is covered by an oxide layer some 20–40 Å thick and indicates that electrolytically polished surfaces also become contaminated. Roscoe's work shows that a layer of 20–40 Å thickness is sufficient to raise appreciably the critical shear stress of cadmium single crystals. The strength of a crystal may be permanently lowered by electrolytic action, as shown by our preliminary results on cadmium and by the work of Harper and Cottrell (1950) on electropolished crystals of zinc. This reduction in mechanical resistance may, perhaps, be attributed to a greater ease with which a travelling dislocation can pass out of a crystal at a perfectly clean surface, in which case it is understandable that further immersion in electrolyte would produce no effect, despite the presence of a film some 20–40 Å thick, in accordance with the results of Harper and Cottrell.

The lack of effect with polycrystalline metal is easily understood on the views that we have put forward, since only the surface grains would be affected, but not on the views of Rehbinder and Wenström (1937), who consider that a deep penetration of the active agent takes place. Grain boundaries would seem to offer great facilities for such action.

ACKNOWLEDGMENTS

Our best thanks are due to Professor H. Terrey, who has helped us by placing his great knowledge of the behaviour of electrolytes at our disposal. One of us (R. F. Y. R.) wishes to acknowledge with gratitude a grant from the Ministry of Supply and to thank Professor W. Sucksmith for providing facilities for the work on zinc in the Department of Physics in the University of Sheffield.

REFERENCES

ANDRADE, E. N. DA C., 1945, *Nature, Lond.*, **156**, 113.
ANDRADE, E. N. DA C., and HENDERSON, C., 1951, *Phil. Trans. Roy. Soc.* A, **244**, 177.
ANDRADE, E. N. DA C., and RANDALL, R. F. Y., 1948, *Nature, Lond.*, **162**, 890; 1950, *Proc. Phys. Soc.* B, **63**, 198.
ANDRADE, E. N. DA C., and ROSCOE, R., 1937, *Proc. Phys. Soc.*, **49**, 152.
HARPER, S., and COTTRELL, A. H., 1950, *Proc. Phys. Soc.* B, **63**, 331.
MENTER, J. W., and HALL, E. O., 1950, *Nature, Lond.*, **165**, 611.
RAETHER, H., 1950, *J. Phys. Radium*, **11**, 11.
REHBINDER, P., and WENSTRÖM. E. K., 1937, *Bull. Acad. Sci. U.R.S.S.*, **4/5**, 531.
RILEY, H. L., and GALLAFENT, V., 1932, *J. Chem. Soc.*, 514.
ROSCOE, R., 1936, *Phil. Mag.*, **21**, 399.

LETTERS TO THE EDITOR

Ferromagnetic Resonance in Manganese Antimonide

Ferromagnetic resonance absorption has been studied in powdered specimens of MnSb at a wavelength of 1·26 cm and in the temperature range from 20°C to the Curie point (315°C). The absorption measurements were performed as previously indicated (Adam and Standley 1950), the powdered specimen under examination being formed into a thin plate, using a suitable low-loss adhesive. The applied steady magnetic field, $H_z^{\max}$, for maximum power absorption was determined at each temperature.

Kittel (1948) has shown that the resonance condition is given by

$$\nu = \frac{ge}{4\pi mc}\left\{(H_z^{\max}+(N_y-N_z)I)(H_z^{\max}+(N_x-N_z)I)\right\}^{1/2}.$$

Here ν is the frequency of the microwave field H_x, g is the spectroscopic splitting factor, N_x, N_y, N_z are the demagnetizing factors of the specimen in the three coordinate directions, and the other symbols have their usual significance. $(N_x-N_z)I$ was found to be negligible in these experiments, and an oscillation magnetometer of the type described by Griffiths and MacDonald (1951) permitted the measurement of the factor $(N_y-N_z)I$ throughout the required temperature range on the actual specimens used in the absorption measurements.

Typical results are shown in the table, and it will be noted that, above about 100°c, as the temperature rises both the g-value determined from the above equation and the half-width of the absorption curve decrease. Five different samples all showed the same behaviour, with only small deviations from the mean values given in the table.

Temperature (°c)	20	65	90	140	170	200	220	250	290
Half-width (Oe)	5000	5500	5700	5600	5000	4000	3300	2500	1100
g	$2{\cdot}7_5$	2·6	2·4	2·2	$2{\cdot}1_5$	$2{\cdot}1_3$	$2{\cdot}1_2$	2·1	2·1

Griffiths (1951) and MacDonald (1951) have shown that anisotropic strains in the specimen modify the above resonance formula, but that the form of the equation remains unaltered if the terms which account for shape anisotropy are written $(N_y'-N_z')I$ and $(N_x'-N_z')I$ and are taken now to include also strain anisotropy. The oscillation magnetometer yields the modified term $(N_y'-N_z')I$, and there is therefore no obvious experimental condition which would account for the observed change in g-value with temperature.

The above results are at variance with those found by Bloembergen (1950) for nickel and supermalloy. In these materials the g-value is unaffected, within experimental error, by temperature changes and the absorption curves broaden appreciably as the temperature is raised. A recently published note by Okamura, Torizuka and Kojima (1951) indicates that results, somewhat similar to those reported here, have been found in cobalt ferrite.

Kittel (1949) and Van Vleck (1950) have shown that spin–orbit interactions can lead to a spectroscopic splitting factor greater than the spin-only value of 2·00. However, in the temperature range from 20°c to 300°c the change in lattice configuration should be small, so that the contribution of the orbital motion to the g-value should not appreciably alter, and hence a constant g-value would be expected. The change in line width with temperature in MnSb and in cobalt ferrite could be explained in terms of a decrease in the anisotropy constant K with increasing temperature. K is not known for MnSb, but if it is high at room temperature (as in MnBi and cobalt ferrite) then the observed decrease in g-value follows the probable decrease of the anisotropy forces. Although the experimental accuracy diminishes near the Curie point, due to reduced absorption, g appears to approach the value 2·1 rather than 2·0. Here the anisotropy forces are expected to be small, and the departure from the spin-only value is similar to that found in such materials as supermalloy and nickel.

Department of Physics,
University of Nottingham.
23rd March 1952.

G. D. Adam.
K. J. Standley.

Adam, G. D., and Standley, K. J., 1950, *Proc. Phys. Soc.* B, **63**, 820.
Bloembergen, N., 1950, *Phys. Rev.*, **78**, 572.
Griffiths, J. H. E., 1951, *Physica*, **17**, 253.
Griffiths, J. H. E., and MacDonald, J. R., 1951, *J. Sci. Instrum.*, **28**, 56.
Kittel, C., 1948, *Phys. Rev.*, **73**, 155; 1949, *Ibid.*, **76**, 743.
MacDonald, J. R., 1951, *Proc. Phys. Soc.* A, **64**, 968.
Okamura, T., Torizuka, Y., and Kojima, Y., 1951, *Phys. Rev.*, **84**, 372.
Van Vleck, J. H., 1950, *Phys. Rev.*, **78**, 266.

Low Remanence and the Temperature Variation of Permeability of Silicon Iron Alloys

According to simple domain theory the remanent intensity of magnetization I_R of a polycrystalline ferromagnetic should have a value equal to $0{\cdot}5\,I_S$ when the material possesses uniaxial anisotropy, and $0{\cdot}83\,I_S$ or $0{\cdot}87\,I_S$ according as the direction of easy magnetization is the [100] or the [111] direction respectively. In most materials these predictions are fairly well supported by experimental observations, but there are some

which possess much lower remanence than that given above. Bozorth (1947) has suggested three possible mechanisms whereby these low values may be brought about, and he considers that the most likely explanation is that in magnetically soft materials the domain wall energy is sufficiently small to allow the substance to demagnetize itself by the formation of new domain boundaries as soon as the applied field is removed, thus giving rise to quite large regions inside the material where the flux is closed to a considerable extent. The greater the extent of this flux closure, the smaller the remanence becomes.

The expression quoted by Bozorth for the wall energy per cm^2 is

$$W=2\left(\frac{3}{2}\lambda\sigma+\frac{K}{3}\right)^{1/2}\left(\frac{k\theta}{a}\right)^{1/2}$$

where λ is the saturation magnetostriction, σ the stress acting on the material, K the magnetocrystalline anisotropy coefficient, k Boltzmann's constant, θ the Curie temperature in degrees Kelvin and a the interatomic distance. From this equation it is evident that W decreases with increasing temperature. Now it is possible that flux closure may occur to a lesser extent even in the presence of a small applied field, and if this mechanism occurs at any stage in the course of magnetization, then at a given field strength the intensity of magnetization will vary with temperature in a manner different from that to be expected when flux closure effects are absent. In particular, if the process occurs to any great extent, the permeability may decrease with temperature in contrast to the behaviour usually observed.

It is to be expected that the materials which would exhibit this effect in the greatest degree would be those for which the saturation intensity, and hence the self-demagnetizing energy, is large, and for which the crystal anisotropy is small. These properties are possessed by the iron-rich Si–Fe alloys.

Measurements made in this laboratory have shown that for 4% Si–Fe the remanence is about 400 gauss, so that $I_R/I_S=0{\cdot}25$. According to Bozorth's figures there are indications that the remanence decreases with increasing silicon content, the ratio I_R/I_S for a 6·5% Si–Fe alloy being only 0·11. Now it is well known that these alloys exhibit an anomalous temperature variation of permeability, the permeability decreasing with temperature at low field strengths in contrast to the behaviour of pure iron in this respect. Spooner (1926) has shown that the addition of silicon to iron causes $d\mu/dT$ to decrease and to acquire negative values at certain inductions, $d\mu/dT$ becoming more negative the greater the silicon content. For example, at room temperature and for $B=10000$ gauss $d\mu/dT$ in gauss per oersted per °C is $-0{\cdot}00012$, $-0{\cdot}0008$, $-0{\cdot}0018$ for silicon–iron containing 0·9% Si, 2·2% Si, and 4% Si respectively. There appear to be no similar measurements for 6·5% Si–Fe, but observations by Zaimovsky (1941) indicate that for 12–14% Si–Fe $d\mu/dT$ is also negative in low fields, and the same worker has found similar behaviour in iron-rich Fe–Si–Al alloys.

These observations suggest that low remanence and negative temperature coefficients of permeability are closely connected and that both can be explained in terms of internal flux closure. The bearing of such a magnetic process on the low field magnetocaloric effect, which would give rise to anomalous temperature changes in low fields of the same sign as the high field effect, has been discussed by Stoner and Rhodes (1949) and has recently been confirmed by Bates and Marshall in unpublished experiments on Si–Fe alloys to be described shortly.

I am indebted to Professor L. F. Bates for his interest and advice and for allowing me to quote the above results prior to publication.

Department of Physics,
University of Nottingham.
19th March 1952.

E. W. Lee.

Bozorth, R. M., 1947, *Z. Phys.*, **124**, 519.
Spooner, T., 1926, *Phys. Rev.*, **27**, 183.
Stoner, E. C., and Rhodes, P., 1949, *Phil. Mag.*, **40**, 481.
Zaimovsky, A. S., 1941, *J. Phys., U.S.S.R.*, **4**, 569.

Strain Patterns in Toughened Glass

When plane polarized light is transmitted by a sheet of toughened glass at large angles of incidence, the strain pattern may be clearly seen without the usual analysing screen or prism. The effect may be observed simply by looking through an inclined sheet of strained glass towards clear sky, and is sometimes noticeable in motor car windscreens.

The Fresnel formulae show that approximately 25% of the light transmitted by a single glass surface is plane polarized for an angle of incidence of 80°. A plate of toughened glass may therefore be considered to contain its own analyser, the glass–air surface, if it is sufficiently inclined to the incident polarized light. An auxiliary, strain-free plate, held parallel to the toughened panel, should augment the analysing effect and increase the contrast under which the pattern may be seen. The two added surfaces would then contribute a degree of polarization intermediate between that found from the Fresnel formulae and the corrected value allowing for internal reflection (Gaviola and Pringsheim 1924, Tuckerman 1947). The corresponding increase in contrast should be roughly twice. Polarization at the front surface of the toughened plate is insufficient, by itself, to lead to the formation of a strain pattern.

Experiments have shown that sufficient contrast is obtained with angles of incidence greater than about 70° for the pattern of a strained glass specimen to be seen in plane polarized light, without the usual analyser. The addition of an auxiliary parallel glass plate has led to a marked increase of the pattern contrast. By rotating the plane of polarization relative to the inclined panel the intensity of illumination has been found to show two maxima and two minima per revolution, at each point of the pattern. This is in accordance with the formula, given by Schuster, $\cos^2(\beta-\alpha)-\sin 2\alpha \sin 2\beta \sin^2 \delta/2$, where α, β are the angles between the optic axis and the directions in the polarizer and analyser respectively and δ is the phase difference. The formula is here modified for the case β=constant, and for points of equal phase difference between components the intensity varies as $j+k\cos 2\alpha+l\sin 2\alpha$, where $j=\frac{1}{2}$ and k and l are constants which depend on the values chosen for β and δ. With incident white light the pattern is coloured in the usual manner.

Field tests have been made with the light reflected from large surfaces such as roads or runways, with skylight at altitudes exceeding 20 000 ft. and with light reflected from layers of light cloud or haze below an aircraft. All tests have shown the importance of the strain pattern effect in oblique windscreens incorporating toughened panels. Very pronounced patterns were observed against layers of thin haze and this effect was still very well marked during twilight. Since analysis occurs at the glass–air surface the effect can only be obviated by lessening the strain pattern in the toughened glass.

Thanks are due to the Chief Scientist, Ministry of Supply, for permission to publish this note.

Royal Aircraft Establishment,
South Farnborough, Hants.
3rd April 1952.

J. M. Naish.
E. R. Webb.

Gaviola, E., and Pringsheim, P., 1924, *Z. Phys.*, **24**, 24.
Schuster, A., 1904, *Theory of Optics* (London : Edward Arnold), p. 181.
Tuckerman, L. B., 1947, *J. Opt. Soc. Amer.*, **37**, 818.

On the Sampling of Water Droplets in Natural Clouds and in Radiation Fogs

In their recent review of the microphysics of clouds, Mason and Ludlam (1951) include a section on the determination of cloud droplet size which calls for certain comments. It may be that some facts escaped the notice of the authors or that they were omitted as being unimportant, but their statement that " a glass slide coated with vaseline or magnesium oxide may be exposed to the cloud elements " suggests an over-simplification of the problem of size determination.

The mixture in which water particles are trapped and entirely confined must fulfil certain requirements, for example its density should be nearly the same as that of water, the matrix must be smooth and highly viscous (Benedicks and Sederholm 1944) but of refractive index different from that of water to ensure good contrast. Pure vaseline, as proposed by the authors, is definitely not suitable as a matrix for slide-surfacing for the following reasons, clearly stated by Houghton and Radford (1938): the surface of the vaseline layer on the glass is not smooth, and when viewed under dark ground illumination it is streaky and irregular, so that some of the captured drops are always distorted and the contrast is very poor. Further, the density of vaseline is 0·873 g/cm³ at 23°C.

The problem of proper surfacing was solved quite satisfactorily by Fuchs and Petrjanoff (1937) who found that good results can be obtained by collecting the droplets on glass slides coated with a freshly melted mixture of light mineral oil and vaseline. The proportion of the ingredients has to be varied according to air temperature and is 3 : 1 at 20°C. It is quite clear that the light mineral oil is the more important ingredient—its refraction is higher than that of the water.

This method was first used in this country by the present writer during his war-time investigations on natural clouds and radiation fogs (Mazur 1943; see also Kraus and Smith 1949, Perrie 1950 and Best 1951). The light mineral oil was previously saturated with distilled water and every effort made to obtain a bubble-free film mixture. In order to avoid a piling-up of droplets into layers when being captured on the plate, the duration of sampling has to be very short. The instrument used was known as the aircraft impactor and consisted essentially of a high-speed shutter with the glass plate covered either with a uniform film of the Fuchs–Petrjanoff mixture or, alternatively, with a magnesium oxide layer on which the impinging droplets made craters.

The water droplets collected within the oil–vaseline mixture can be preserved for many hours without showing any perceptible diminution in size or change of shape.

The method adopted for the collecting of drops in natural clouds was to coat the cover glasses with the fresh mixture just before the aircraft take-off and then to warm them before use in flight by putting them on to the flat surface of a lagged vessel filled with hot water at about 45–50°C.

Some authors have obtained satisfactory results using other mixtures: (1) Häuser and Strobl (1924) used neat's-foot oil and glycerine; (ii) Diem (1942) used two layers of different oils of different densities, collecting the drops on the interface between the layers; (iii) Bricard (1939) used mineral oil to which organic acids had been added in order to reduce the surface tension to render easier penetration.

The magnesium oxide method is only a modification of the method developed by Strazhevsky (1937), who used a uniform layer of soot smoked on to a slide during his investigation on the atomization of liquid fuel. The magnesium oxide layer is very fragile and can be damaged by high-velocity air jets during exposure to the droplets. The author found that the oxide layer is blown off the plate at a speed of about 200 m.p.h. The method is of little value for droplets smaller than 10 μ.

Incidentally Pauthenier and Brun (1940), mentioned by the authors, have also used the well-known 'stain' or 'absorbent paper' method.

British Rayon Research Association, J. Mazur.
Manchester.
9th November 1951.

Benedicks, C., and Sederholm, P., 1944, *Ark. Mat. Astr. Fys.*, **30A**, No. 6, and **30B**, No. 5; 1944, *Nature, Lond.*, **153**, 80.
Best, A. C., 1951, *Quart. J. R. Met. Soc.*, **77**, 418.
Bricard, 1939, *La Météorologie*, **15**, 83.
Diem, M., 1942, *Ann. Hydrogr., Berlin*, **70**, 142.
Fuchs, N., and Petrjanoff, J., 1937, *Nature, Lond.*, **139**, 111.
Häuser, F., and Strobl, G. M., 1924, *Z. Tech. Phys.*, **5**, 154.
Houghton, H. G., and Radford, W. H., 1938, *Pap. Phys. Oceanogr. Met.*, **6**, No. 4.
Kraus, E. B., and Smith, B., 1949, *Aust. J. Sci. Res.* A, **2**, 376.
Mason, B. J., and Ludlam, F. H., 1951, *Rep. Prog. Phys.*, **14**, 159 (London : Physical Society).
Mazur, J., 1943, *Air Ministry, Met. Res. Committee*, M.R. 109.
Pauthenier, M., and Brun, E., 1940, *C. R. Acad. Sci., Paris*, **211**, 295; *Ibid.*, **212**, 1081.
Perrie, D. W., 1950, *Cloud Physics* (Toronto : University Press), p. 16.
Strazhevsky, L., 1937, *J. Tech. Phys., U.S.S.R.*, **4**, 978.

The Dispersion of Electron Beams in Gases

When a beam of electrons passes through a gas it is scattered mainly elastically, because self-repulsion (Watson 1927) is negligible. The size of a spot produced by the diffuse beam on a fluorescent screen can be measured by a radius r_1 (in cm) which corresponds to a point on the screen having $1/e$ of the intensity at its centre (Lenard 1927); theoretically

$$r_1 = c(pd)^{1/2}d/V_a. \qquad \ldots\ldots (1)$$

Here c (of order 10^3 for N_2) depends on the gas, p is the pressure in mm Hg, V_a the accelerating potential in volts and d the distance travelled in cm. For $p > 10^{-2}$ and $V_a = 10^3 \ldots 10^4$ a spot should not form.

It was found very early that ionization by an electron beam in a rarefied gas (e.g. in He or A) concentrates the beam (Arnot 1930, 1931, Cosslett 1950). A treatment of this 'gas-focusing' was not very successful and the general results could not be compared with experiment (Scherzer 1933). In all these cases (Brüche 1932) the gas pressure used never exceeded 10^{-2} mm Hg and this has been accepted as a practical upper limit. Fortunately this conclusion was unjustified.

We have discovered that an electron beam accelerated to 3–10 kv in nitrogen remains well concentrated even at pressures of about 1 mm Hg. We believe that 1 mm Hg does not represent an upper limit and that the nature of the gas is not critical.

The ultimate cause of the concentration of the beam is the presence of positive ions in and around the beam. The fast electrons produce at this pressure a small number of ion pairs along the path of the beam. The slow secondary electrons and positive ions so formed diffuse radially outwards. The electrons, being originally faster than the ions, set up a distribution of concentration such that at the axis of the beam the concentration of ions slightly exceeds that of the electrons; as a result a positive net space charge develops. Since secondary electrons and ions are produced in equal numbers, a negative net charge develops at larger radii. At still greater radii the relative velocities of electrons and ions become so small that the particles recombine readily in the gas and their concentration decreases more rapidly. As the space-charge distribution develops the radial velocities of electrons become smaller and those of the ions larger. In equilibrium their speeds at a given radius are equal and so are the numbers crossing the corresponding cylindrical surface. In the following arguments the effect of the negative space charge due to the fast electrons is neglected.

We have made some rough calculations in order to test whether this picture gives consistent results. The condition to be satisfied is that the net positive charge in the beam is large enough to restrain the fast electrons from being scattered out of the beam. In addition we have to assume that the average random velocity of the secondary electrons is larger than the corresponding velocity of the fast electrons.

An electron of energy 5 kev produces about 1 ion pair per cm at 1 mm Hg (von Engel and Steenbeck 1932). Thus with a beam current of 1 microampere, 6×10^{12} ion pairs are produced per sec per cm length of the beam. If the loss by ambipolar diffusion is balanced against this rate of production the equilibrium concentration found is of order 10^{11} ion pairs/cm^3. A similar value is obtained if the concentration is determined by balancing recombination against diffusion, using a recently measured value for the coefficient of recombination (Biondi and Brown 1949). The above value of the concentration is large enough to justify the assumption of ambipolar diffusion (Loeb 1939). At the same time it is not excessive and thus the concentrations of positive ions can be slightly different from that of the electrons. This is particularly likely to occur at the core of the beam.

If ambipolar diffusion operates, the net positive charge should be only a fraction of the total charge present. We have calculated therefore the space charge needed by assigning to the primary beam an average energy of random motion of order 10 ev, a value which can be obtained from the classical treatment of elastic scattering. Since the beam has a radius of less than 1 mm the potential at this radius must be about 10 v negative with respect to the axis if the fast electrons are to be retained within a beam of that radius. The space charge density which gives this potential is of order 10^{11} ions/cm^3. These results appear to be consistent and reasonable.

The axial motion charges depend on the potential of the isolated screen with respect to the anode. In high vacuum this potential may be large (McKeag and Welch 1951, McKay 1948) but in a gas the screen potential must be so small that the radial charge distribution is not disturbed.

Gas focusing at low pressure is a fundamentally different phenomenon. The radial motion of the secondaries occurs essentially in a vacuum and so the walls become important (Arnot 1930).

The permission is acknowledged of the Director of the Electrical Research Association to publish this note. Professor Lord Cherwell has kindly placed the facilities of this laboratory at our disposal.

Clarendon Laboratory, P. F. Little.
Oxford University. A. von Engel.
28th March 1952.

Arnot, F. L., 1930, *Proc. Roy. Soc.* A, **129**, 261; 1931, *Proc. Camb. Phil. Soc.*, **27**, 73.
Biondi, M. A., and Brown, S. C., 1949, *Phys. Rev.*, **76**, 1697.
Brüche, E., 1932, *Z. Phys.*, **78**, 177.
Cosslett, V. E., 1950, *Electronic Optics* (Oxford : University Press).
von Engel, A., and Steenbeck, M., 1932, *Elektrische Gasentladungen* I (Berlin : Springer).
Lenard, P., 1927, *Handbuch Exp. Phys.* (Leipzig : Akad. Verh.).
Loeb, L. B., 1939, *Fundamental Processes of Electrical Discharge in Gases* (New York: Wiley).
McKay, K. G., 1948, *Advances in Electronics* (New York : Academic Press).
McKeag, A. H., and Welch, E. E., 1951, *Industr. Engng. Chem.* **27**, 110.
Scherzer, O., 1933, *Z. Phys.*, **82**, 697.
Watson, E. E., 1927, *Phil. Mag.*, **3**, 849.

Microwave Faraday Rotation in Liquid Oxygen

Observations of the microwave Faraday effect have been reported by various workers (see references) on paramagnetic and ferromagnetic materials, and theoretical discussions of the ferromagnetic case have been given by the present writer (1951) and by Hogan (1952). Oxygen gas and liquid are well known to be paramagnetic, and it has been of interest in connection with rotation measurements on other substances at liquid oxygen temperature to know what contribution might be made to the observations by atmospheric oxygen in the waveguide. The expression given previously (Roberts 1951) for the rotation in ferromagnetics may be applied to paramagnetics within the same approximations provided that we use the appropriate value for the intensity of magnetization (in the applied field). Thus in a field of 1 000 oersteds we estimate for liquid oxygen just below its boiling point at atmospheric pressure (assuming a dielectric permittivity of about 1·5) a rotation of about 0·6 deg/cm. Measurements in these Laboratories with sample lengths of about 15 cm at a frequency of 10 kMc/s have failed to show any rotation as great as 0·2% of this estimate, either for the liquid or for gaseous O_2 just above its boiling point.

The almost complete suppression of the Faraday effect in this case may be attributed to the very strong magnetic damping of the spin precession caused by the molecular collisions. Such collisions will be exceptionally effective in the case of the oxygen molecule in the microwave frequency range, on account of the inherent (magnetic) molecular resonance which occurs at about 60 kMc/s.

Post Office Research Station, F. F. Roberts.
Dollis Hill, London.
24th April 1952.

Gozzini, A., 1951, *Nuovo Cim.*, **8**, 928.
Hogan, C. L., 1952, *Bell Syst. Tech. J.*, **31**, 1.
Roberts, F. F., 1951, *J. Phys. Radium*, **12**, 305.
Soutif-Guicherd, J., and Lambinet, M., 1950, *C.R. Acad Sci., Paris*, **231**, 1460.
Wilson, M. C., and Hull, G. F., 1948, *Phys. Rev.*, **74**, 711.

The Influence of Heat Treatment on Magnetic Viscosity in Permanent Magnet Alloys

In the development of the magnetic properties of dispersion hardened permanent magnet alloys, the usual form of heat treatment consists of quenching the material from about 1 300° c in air or water and then maintaining it at a lower annealing temperature of about 650° c for a period of 2 to 4 hours (Bates 1951). The alloys are stable in a single phase system at 1 300° c, but have a transition temperature, which lies between 700° and 900° c, below which a two-phase system is the most stable form. Thus in the case of Fe_2NiAl, which may be considered as the prototype of many permanent magnet alloys, Bradley and Taylor (1938) have shown that a single body centred phase of Fe_2NiAl is stable above 900° c. Below 800° c the alloy tends to form a two-phase system, the component phases both being body centred and having the approximate compositions FeNiAl and Fe. In the normal heat treatment of these alloys, the two phases have insufficient time to separate completely but occur in the material as islands or as small inclusions. It is the presence of the inclusions which most probably accounts for the high coercivities of the alloys (Néel 1946).

The metallurgical processes which occur during this type of heat treatment can be envisaged in terms of the two mechanisms reviewed by Fisher, Hollomon and Turnbull (1948), viz. (*a*) nucleation, that is, the formation of nuclei in the parent matrix from which the inclusions may eventually develop and (*b*) the growth of nuclei into islands and inclusions. The considerations of Fisher *et al.* show that to a first approximation, during a sufficiently

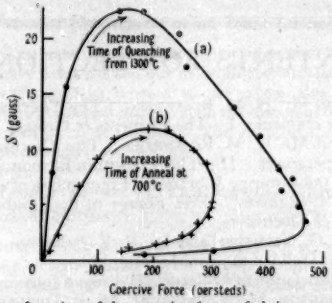

Variation of S as a function of the coercive force of alnico specimens subjected to heat treatments (*a*) and (*b*) described in text.

rapid quench from 1 300° c, only process (*a*) occurs to any significant extent. During the subsequent anneal the conditions are such as to inhibit the formation of new nuclei but the growth of existing nuclei, process (*b*), is favoured. To a good approximation, therefore, the number of inclusions and their size can be independently controlled by the type of quench and time of anneal respectively.

The coercive force of a specimen is a function of the product of the size and number of the inclusions (Néel 1946) and consequently, it is to be expected that widely differing types of heat treatment can lead to the production of specimens of the same coercive force. This behaviour is observed with alnico, e.g. the same coercive force can be achieved either by a relatively slow quench from 1 250° c, or by a rapid quench in cold water followed by an annealing period at 700° c. On the other hand, the phenomenon of magnetic viscosity in an alnico specimen is a unique function of the previous heat treatment. The magnetic viscosity may be described in terms of the parameter S defined in a previous paper (Street and Woolley 1949) in which it is shown that the time variation of intensity of magnetization ΔI of alnico specimens is of the form $\Delta I = S \ln t + \text{constant}$. In this expression, t is the time which has elapsed after a sudden change in the magnetic field applied to the specimen has been made.

The figure shows the results of measurements of S and H_c on alnico specimens which were subjected to two different types of heat treatment: (*a*) cooled from 1250° c at different rates, varying from water quenching to cooling the specimen at the natural rate of cooling of

the furnace with the current switched off; (*b*) cold water quench followed by successive anneal at 700° c for various total times varying from 5 minutes to 140 hours.

Work on the lines indicated above is proceeding with a view to explaining the observed phenomena in terms of the nucleation theory of precipitation from solid solution. It is hoped to publish an account of this work at a later date.

A further point arises from the results given in the figure, which extend the rather similar measurements which have been briefly reported by Bulgakov and Kondorskii (1949). In the latter work, it is concluded that the smaller the coercive force of alnico the greater is the magnetic viscosity. The present results show that this statement is only true for values of coercive force exceeding about 150 oersteds. From the figure it can be seen that specimens of coercive force smaller than 150 oersteds have, in fact, smaller magnetic viscosity the smaller the coercive force.

Department of Physics,
University of Nottingham.
15th April 1952.

R. Street.
J. C. Woolley.
P. B. Smith.

Bates, L. F., 1951, *Modern Magnetism* (Cambridge : University Press, 3rd edn.), p. 94.
Bradley, A. J., and Taylor, A., 1938, *Magnetism* (London : Institute of Physics), p. 89.
Bulgakov, N., and Kondorskii, E., 1949, *Dokl. Akad. Nauk, S.S.S.R.*, **69**, 325.
Fisher, J. C., Hollomon, J. H., and Turnbull, D., 1948, *J. Appl. Phys.*, **19**, 775.
Néel, L., 1946, *Ann. Univ., Grenoble*, **22**, 299.
Street, R., and Woolley, J. C., 1949, *Proc. Phys. Soc.* A, **62**, 562.

CONTENTS FOR SECTION A

PAGE

Dr. K. Mendelssohn and Mr. H. M. Rosenberg. The Thermal Conductivity of Metals at Low Temperatures : I—The Elements of Groups 1, 2 and 3 . . 385
Dr. K. Mendelssohn and Mr. H. M. Rosenberg. The Thermal Conductivity of Metals at Low Temperatures : II—The Transition Elements. 388
Dr. M. Blackman. On the Limiting Vibrational Frequencies of an Ionic Lattice . 394
Dr. S. Levine and Mr. A. Suddaby. Free Energy of the Double Layers of Two Parallel Plates in a 1–2 Electrolyte 405
Dr. A. Lagerqvist, Mr. G. Nilheden and Dr. R. F. Barrow. The Near Ultra-Violet Band-System (D–X) of Silicon Monosulphide 419
Dr. K. E. A. Effat. Dissociation of Molecular Hydrogen Ions in the Cyclotron . 433
M. J. Becker, M. P. Chanson, M. E. Nageotte, M. P. Treille, Mr. B. T. Price and Miss P. Rothwell. The Increase of Ionization with Momentum for Energetic Cosmic-Ray Particles 437
Letters to the Editor :
Dr. J. Walker. ^{83}Kr—The Possible Existence of a Nuclear Level preceding the Metastable State 449
Dr. P. T. Barrett. ^{83}Kr—An Investigation of the Radiations succeeding the Metastable State 450
Dr. R. J. Blin-Stoyle. A Note on Time Reversal in Polarized Nuclear Processes 452
Dr. M. J. Poole. Neutron Flux and Spectrum Measurement 453
Mr. D. H. Simmons. The Range–Energy Relation for Protons in Aluminium. 454
Dr. M. A. Grace, Mr. H. R. Lemmer and Dr. H. Halban. The Response of a NaI Scintillation Counter to Slow and Fast Neutrons 456
Dr. R. G. Chambers. The Kinetic Formulation of Conduction Problems . 458
Dr. R. B. Potts. A Combinatorial Problem in Electron–Photon Cascade Theory 459
Dr. J. S. Blakemore. The Parameters of Partially Degenerate Semiconductors 460
Mr. W. R. S. Garton. Schumann Region Absorption Spectrum of Copper Vapour 461
Contents for Section B. 462
Abstracts for Section B 463

ABSTRACTS FOR SECTION A

The Thermal Conductivity of Metals at Low Temperatures: I—The Elements of Groups 1, 2 *and* 3, by K. MENDELSSOHN and H. M. ROSENBERG.

ABSTRACT. The thermal conductivity of Cu, Ag, Au, Mg, Cd, Al, In and one polycrystalline and two single crystal specimens of Zn have been measured in the range 2–40° K. Each specimen shows a maximum in the conductivity in this range. The values of the coefficients α and β in the equation for the thermal resistance $R=\alpha T^2+\beta/T$ have been calculated for each specimen.

The Thermal Conductivity of Metals at Low Temperatures: II—The Transition Elements, by K. MENDELSSOHN and H. M. ROSENBERG.

ABSTRACT. The thermal conductivity in the range 2–40°K has been measured for Ti, Mn, Fe, Ni, Zr, Cb, Mo, Rh, Pd, Ta, W, Ir, Pt, U, and for a Pb single crystal. As a rule, the metals of group 8 have a much higher conductivity than have the metals of the earlier groups. The values of α and β in the equation for the thermal resistance $R=\alpha T^2+\beta/T$ have been calculated for each specimen. The experiments on Cb indicate that the normal state was not reached in a field of 3300 gauss at temperatures below 5°K.

On the Limiting Vibrational Frequencies of an Ionic Lattice, by M. BLACKMAN.

ABSTRACT. The vibrational frequencies of an orthorhombic ionic lattice, of the thallium fluoride type, have been worked out in detail for wavelengths long compared with the crystal spacing though short in relation to the crystal size. It is shown that these frequencies are not unique but depend in general on the direction of the wave in the crystal—in contrast to what happens in cubic crystals. The effect of this behaviour on the vibrational spectrum is discussed briefly.

Free Energy of the Double Layers of Two Parallel Plates in a 1–2 *Electrolyte*, by S. LEVINE and A. SUDDABY.

ABSTRACT. By making use of the Poisson–Boltzmann equation an expression is obtained for the free energy of the electric double layers of two parallel plates immersed in a large volume of an electrolyte of the 1–2 valency type. Two cases arise depending on whether or not the divalent ion and the surface charge have the same sign. The formula for the free energy is expressed in terms of elliptic integrals. An approximate form for the free energy, which is more convenient for numerical computations, is also obtained. This is particularly suitable at large surface potentials and is derived for a symmetrical electrolyte as well as for the asymmetrical ones. Numerical tables of the free energy as a function of plate separation are given and some applications are briefly indicated.

The Near Ultra-Violet Band System (D–X) of Silicon Monosulphide, by A. LAGERQVIST, G. NILHEDEN and R. F. BARROW.

ABSTRACT. The rotational analysis of the near ultra-violet band-system, $D\,^1\Pi-X\,^1\Sigma^+$, has been extended. Twelve bands have been analysed, namely, the 7,1, 6,0, 6,1, 5,0, 5,1, 4,0, 4,1, 3,0, 2,0, 1,0, 1,1 and 0,0 bands. The constants derived for $D\,^1\Pi$ are

$$B_{v'}=0{\cdot}2664_7-0{\cdot}0021_6(v'+\tfrac{1}{2});\ D_{v'}=[2{\cdot}91-0{\cdot}03(v'+\tfrac{1}{2})]\times10^{-7},$$
$$G_{v'}=513{\cdot}1_2(v'+\tfrac{1}{2})-2{\cdot}9_3(v'+\tfrac{1}{2})^2;\ \nu_e=35026{\cdot}8_6\ \text{cm}^{-1};\ r_e'=2{\cdot}058_9\ \text{Å}.$$

A number of perturbations have been found in the upper state. They appear to arise from interactions with two electronic states, a $^3\Sigma^-$ state and a singlet state, $^1\Pi$ or $^1\Delta$. It has not been possible to determine the absolute numbering of the vibrational levels of the perturbing states, but in all other respects fairly complete information has been obtained about the $^3\Sigma^-$ state. The perturbations are similar to those already known in the spectrum of CO, and the analogy between the electronic states of the molecules is thus strengthened.

Dissociation of Molecular Hydrogen Ions in the Cyclotron, by K. E. A. Effat.

ABSTRACT. The dissociation of H_2^+ ions by collision with gas molecules greatly reduces the current of these ions that can be obtained from a cyclotron. The current has been measured at two distances from the ion source corresponding to energies of 9 and 18 Mev and with various pressures of air and argon in the tank; the loss of ions in expanding from the smaller to the larger radius is somewhat less than is predicted by Salpeter's calculations of the dissociation cross section. Assuming this cross section to be inversely proportional to the kinetic energy of the ion, the product σE is found experimentally to be $(1{\cdot}9 \pm 0{\cdot}4) \times 10^{-18}$ cm² Mev per 'atom' of air and $(7{\cdot}0 \pm 1{\cdot}4) \times 10^{-18}$ cm² Mev per atom of argon.

The Increase of Ionization with Momentum for Energetic Cosmic-Ray Particles, by J. Becker, P. Chanson, E. Nageotte, P. Treille, B. T. Price and P. Rothwell.

ABSTRACT. An experiment is described in which the momentum and specific ionization of cosmic-ray mesons were simultaneously measured, the momentum by means of a cloud chamber in a magnetic field, and the specific ionization by rectangular proportional counters. The difficulties inherent in the use of proportional counters for such measurements are discussed.

The experimental results are in satisfactory agreement with theoretical predictions of an increase of specific ionization for very energetic μ-mesons.